Journal of Nuclear Medicine, published on April 6, 2018 as doi:10.2967/jnumed.118.210443

Development of quinoline based theranostic ligands for the targeting of fibroblast activation protein

Thomas Lindner[1*], Anastasia Loktev[1,2,6*], Annette Altmann[1,2], Frederik Giesel[1], Clemens Kratochwil[1], Jürgen Debus[3,4], Dirk Jäger[5], Walter Mier[1], Uwe Haberkorn [1,2§]

(1) Department of Nuclear Medicine, University Hospital Heidelberg, Heidelberg Germany.
(2) Clinical Cooperation Unit Nuclear Medicine, German Cancer Research Center (DKFZ), Heidelberg, Germany.
(3) Dept. of Radiation Oncology, University Hospital Heidelberg, Heidelberg, Germany
(4) Clinical Cooperation Unit Radiation Oncology, German Cancer Research Center (DKFZ), Heidelberg, Germany
(5) Dept. of Medical Oncology, National Center for Tumor Diseases (NCT), Heidelberg, Germany
(6) Faculty of Biosciences, Heidelberg University

*****Authors contributed equally.

§ Corresponding author:

Uwe Haberkorn
Department of Nuclear Medicine
University Hospital Heidelberg
Im Neuenheimer Feld 400
69120 Heidelberg
Tel: +49-6221-56-7732
Fax: +49-6221-56-5473
Email: Uwe.Haberkorn@med.uni-heidelberg.de

First author:
Thomas Lindner
Department of Nuclear Medicine
University Hospital Heidelberg
Im Neuenheimer Feld 400
69120 Heidelberg
Tel: +49-6221-56-7726
Fax: +49-6221-56-5473
Email: Thomas.Lindner@med.uni-heidelberg.de

Conflicts of interest: Patent application (EP 18155420.5) for quinolone based FAP targeting agents for imaging and therapy in nuclear medicine (UH, AL, TL and WM).

Word count: 4971

ABSTRACT

Fibroblast activation protein (FAP) is overexpressed in cancer associated fibroblasts and is involved in a variety of tumor promoting activities such as matrix remodeling, angiogenesis, chemotherapy resistance and immunosuppression. Since FAP shows low expression in most normal organs it presents an interesting target for imaging and endoradiotherapy. In this paper, FAP inhibitors were modified and optimized for their use as theranostic tracers.

Methods: FAP inhibitors (FAPIs) based on a quinoline structure were synthesized and characterized with respect to binding, internalization and efflux in cells expressing human and murine FAP as well as CD26. Preclinical pharmacokinetics were determined in tumor bearing animals with biodistribution experiments and small animal positron emission tomography (PET). Finally, a proof of concept approach of imaging and therapy was chosen in two patients with metastasized breast cancer.

Results: Of 11 synthesized FAPIs FAPI-04 was identified as the most promising tracer for clinical application. Compared to the previously published ligand FAPI-02, FAPI-04 showed an excellent stability in human serum, a higher affinity for FAP as opposed to dipeptidyl peptidase 4 and a slower excretion in vitro. In vivo, a higher SUV was reached in tumor-bearing animals leading to higher area under curve values calculated from biodistribution experiments. Finally, PET/CT scans with ^{68}Ga-FAPI-04 in two patients with metastasized breast cancer revealed high tracer uptake in metastases and a reduction of pain symptoms after therapy with a considerable low dose of ^{90}Y-FAPI-04.

Conclusion: FAPI-04 represents a promising tracer for both diagnostic imaging and possibly targeted therapy of malignant tumors with a high content of activated fibroblast such as breast cancer.

INTRODUCTION

Cancer-associated fibroblasts are known as modulators of the microenvironment of malignant tumors which act by secreting factors that regulate malignant cells as well as non-malignant cells such as immune cells and endothelial cells (*1*). Although heterogeneous in their origin, cancer-associated fibroblasts have common properties which are distinct from normal fibroblasts and show expression of proteins not found in their normal counterparts. One of these proteins is the fibroblast activation protein (FAP), a type II transmembrane serine protease with both a dipeptidyl peptidase and an endopeptidase activity (*2-4*).

FAP expression has been found to be associated with a poor prognosis in a variety of tumors such as colon (*5*), pancreatic (*6*), ovarian (*7*) and hepatocellular carcinoma (*8*). It plays multiple biological roles in cancer. First, via its peptidase activity FAP leads to matrix digestion and remodeling of the tumor microenvironment enabling invasion and migration of tumor cells (*9*). Since neuropeptide Y is a natural substrate of FAP and the cleavage product has been shown to be proangiogenic, FAP is considered to be involved in tumor angiogenesis. This is substantiated by studies showing a correlation between FAP expression and microvessel density in tumors (*10,11*).

Furthermore, besides its enzyme function FAP activates cell signaling by forming complexes with other proteins, for example β1 integrins such as $\alpha 3\beta 1$ (*12,13*).

Since cancer-associated fibroblasts are the primary source of collagen I which contributes to decreased chemotherapeutic drug uptake and thereby plays a role in regulating the sensitivity of tumors towards chemotherapy, elimination of these fibroblasts via targeting of FAP may lead to increased uptake of chemotherapeutic drugs and greater therapeutic efficiency (*14*). Finally, an immunosuppressive role has been described (*15*).

In addition, FAP has other favorable properties qualifying it as a promising target for diagnosis and therapeutic intervention: besides expression in some non-malignant conditions such as wound

healing, rheumatoid arthritis, artherosclerotic plaques, and diseases leading to fibrosis it is expressed in more than 90% of human epithelial cancers, is absent in human adult normal tissues and has a large extracellular domain with the catalytic site also located extracellularly. These properties ensure a low background activity with a high image contrast and a low frequency of side effects for FAP targeting molecules, the possibility of application in many different tumor entities and the design of combination therapies targeting both tumor cells and the stromal components of a tumor. Such targeting of the stromal cells has been done using a variety of molecules including antibodies (*16-18*), chimeric antigen receptor T cells (*19,20*), immunoconjugates (*21*), peptide-drug complexes bearing the consensus sequence for the enzymatic activity (*22,23*), vaccines (*14,24*) and small molecules for the inhibition of FAP enzyme activity (*25*). Another approach is the use of these small molecules as carriers of radioactivity into the tumor for both imaging and therapy. In a previous paper we showed that FAPI-02 rapidly accumulated in FAP-expressing cells, tumor xenografts and in patients (*26*). Although a high image contrast was obtained, the tumor retention time was relatively short, which presents no problem for diagnosis, but may need improvement for therapy. In this paper we designed variants of FAPI-02 with the goal to increase tumor retention time and thereby to develop a theranostic FAP-targeting agent.

MATERIALS AND METHODS

Synthesis and Radiolabeling

The synthetic pathway towards the FAPI derivatives is given exemplary for FAPI-04 (Supplemental Fig. 1). A detailed compilation of the precursors, intermediates and their syntheses can be found in the supplementary information. ^{177}Lu and ^{68}Ga were chelated after pH adjustment with sodium acetate. The reaction mixture was heated to 95 °C for 10 min and completeness of reaction checked by radio liquid chromatography. The ^{68}Ga compounds were processed by solid phase extraction prior to positron emission tomography (PET). Stability in human serum was determined by precipitation of samples and

radio-chromatographic analysis of the supernatant. The stability of the compounds was checked exemplary for FAPI-04 by incubation in human serum at 37 °C (Supplemental Fig. 2).

Cell Culture

HT-1080 cells which are transfected with the human FAP-gene, muFAP and CD26 transfected human embryonic kidney cells (obtained from Stefan Bauer NCT Heidelberg (*27*)) were cultivated in Dulbecco's modified Eagle's medium containing 10% fetal calf serum at 37°C/5% carbon dioxide.

For radioligand binding studies, cells were seeded in 6-well plates and cultivated for 48 h to a final confluence of approx. 80-90% ($1.2–2×10^6$ cells/well). The medium was replaced by 1 mL fresh medium without fetal calf serum. The radiolabeled compound (^{177}Lu-labelled FAPIs; specific activity 200 nmol/GBq) was added to the cell culture and incubated for different time intervals ranging from 10 min to 24 h. Competition experiments were performed by simultaneous exposure to unlabeled (10^{-5} M to 10^{-9} M) and radiolabeled compound for 60 min. In all experiments, the cells were washed twice with 1 mL phosphate-buffered saline pH 7.4 and subsequently lysed with 1.4 ml lysis buffer (0.3 M NaOH, 0.2% SDS). Radioactivity was determined in a γ-counter (Cobra II, Packard), normalized to 10^6 cells and calculated as percentage of the applied dose (%ID). Cell efflux was determined after incubation of the cells with the tracer for 60 minutes. Thereafter, the radioactive medium was removed, cells were washed and incubated in nonradioactive medium for 1, 2, 4 and 24 hours. After washing twice, the cells were lysed and the radioactivity counted. Each experiment was performed 3 times, and 3 repetitions per independent experiment were acquired.

For internalization experiments the cells were incubated with the radiolabeled compound for 60 min at 37 °C and 4 °C. Cellular uptake was terminated by removing medium from the cells and washing twice with 1 mL phosphate-buffered saline. Subsequently, cells were incubated with 1 mL of glycine-HCl (1 M, pH 2.2) for 10 min at room temperature to remove the surface bound activity. The cells were washed with 2 mL of ice-cold phosphate-buffered saline and lysed with 1.4 mL of lysis buffer to determine the

internalized fraction. For the cells incubated at 4 °C, all washing and elution steps were carried out using ice-cold buffers. The radioactivity was measured using a γ-counter, normalized to 1 mio cells and calculated as percentage of applied dose (%ID).

Animal Studies

For *in vivo* experiments, 8 week old BALB/c *nu/nu* mice (Charles River) were subcutaneously inoculated into the right trunk with 5×10^6 HT-1080-FAP cells. When the size of the tumor reached approximately 1 cm^3, the radiolabeled compound (^{177}Lu-labelled FAPIs; specific activity 200 nmol/GBq) was injected via the tail vein. For organ distribution, the animals (n = 3 for each time point) were sacrificed after the indicated time points (from 30 min to 24 h). The distributed radioactivity was measured in all dissected organs and in blood using a γ-counter (Cobra Autogamma, Packard). The values are expressed as percentage of injected dose per gram of tissue (%ID/g). PET imaging was performed using a small-animal PET scanner (Inveon, Siemens). Mice were injected with ^{68}Ga-FAPI-02 (80 nmol/GBq). Within the first 60 min a dynamic scan was performed, followed by a static scan from 120 to 140 min after injection. Images were reconstructed iteratively using the 3D-OSEM+MAP method (Siemens) and were converted to standardized uptake value (SUV) images. Quantification was done using a ROI technique and expressed as SUV. Imaging was also done in animals bearing SK-LMS-1 tumors, a model where the tumor cells are FAP-negative and only activated mouse fibroblasts are present. Blocking experiment was performed by adding 30 nmol unlabeled precursor to the solution of ^{68}Ga-FAPI-04 prior to injection. All animal experiments were conducted in compliance with the German animal protection laws.

Clinical PET/CT-Imaging

Diagnostic imaging of 2 patients was performed under the conditions of the updated declaration of Helsinki, § 37 (unproven interventions in clinical practice) and in accordance to the German

Pharmaceuticals Law §13 (2b) for medical reasons using ^{68}Ga-FAPI-04, which was applied intravenously (80 nmol/GBq), 10 min, 1 and 3 hours post tracer administration. The PET/CT scans were performed with a Biograph mCT Flow™ PET/CT-Scanner (Siemens Medical Solutions) using the following parameters: slice thickness of 5 mm, increment of 3-4 mm, soft-tissue reconstruction kernel, care dose. Immediately after CT scanning, a whole-body PET was acquired in 3D (matrix 200x200) in FlowMotion™ with 0.7 cm/min. The emission data were corrected for random, scatter and decay. Reconstruction was conducted with an ordered subset expectation maximisation (OSEM) algorithm with 2 iterations/21 subsets and Gauss-filtered to a transaxial resolution of 5 mm at full-width half-maximum. Attenuation correction was performed using the low-dose non-enhanced CT data. The quantitative assessment of standardized uptake values (SUV) was done using a region of interest technique. All patients signed written informed consent. The evaluation was approved by our institutional ethical review board (No. S-016/2018).

Therapeutic Application

One patient with metastasized breast cancer was treated with 2.9 GBq of ^{90}Y-FAPI-04 (24 nmol/GBq). FAPI-04 was labeled with a ^{90}Y-chloride solution (Yttriga, Eckert & Ziegler Radiopharma GmbH, Berlin, Germany) and injected intravenously via a low-protein-binding sterile filter system (Filtropur S 0.2, Sarstedt, Nuembrecht, Germany). Gamma camera images of the Bremsstrahlung were acquired 3 h and 1 d after tracer administration using a GE Hawkeye SPECT/CT system.

RESULTS

Synthesis/Radiolabeling

Following the synthetic pathway shown in Supplemental Fig. 1 a total of eleven new compounds and a small molecule-peptide conjugate were synthesized. An overview of the synthesized compounds is given in Fig. 1. To trace the peptide via radioactive labeling, ε-DOTA-lysine was inserted C-terminally between the end of the NLS-sequence and the conjugated cysteine residue

Cell Based Experiments

To evaluate the binding and internalization properties of the FAPI derivatives, radioligand binding assays were performed using FAP-expressing HT-1080 cells (Fig. 2). All tracers showed an almost complete internalization with values over 90%. Due to insufficient binding to human FAP after 24 h, the compounds FAPI-06, -07, -08 and -09 were not characterized further. Although they showed acceptable accumulation after 24 hours, the evaluation of FAPI-11 and -12 was not pursued due to bad performance after 1 and 4 h of incubation. To verify the target specificity, binding assays were also performed using human embryonic kidney cells expressing murine FAP and dipeptidyl peptidase 4 (CD26), which show a high homology to human FAP (see Supplemental Fig. 2). In these experiments FAPI-02 and FAPI-04 showed a strong binding to muFAP with significantly higher values for FAPI-04 and no binding to CD26. However, FAPI-15 also had a low affinity to CD26. Calculation of the ratio muFAP binding/CD26 binding revealed values of 45, 750 and 38 for FAPI-02, FAPI-04 and FAPI-15, respectively (Supplemental Fig. 2).

In the first set of proceeding experiments the difluoroproline-analogs FAPI-04 and -05 were analyzed to investigate the influence of the presence of fluorine as well as the difference between a propyl and a butyl-linkage of the piperazine and quinoline components of the radiotracers. For this purpose, the EC_{50}-values of the inhibitors were determined by competition assays demonstrating a higher target specificity of FAPI-04 (6.5 nM) compared to -05 (17.2 nM; see Supplemental Fig. 3). Efflux experiments show that FAPI-04 and -05 get excreted considerably slower than FAPI-02, resulting in increased half-lives of 3.0 and 2.8 h (FAPI-02: 1.7 h; see Supplemental Fig. 4). FAPI-13 was characterized in more detail due to its resemblance to the compound FAPI-04 and showed the lowest EC_{50}-value in this set of data (4.5 nM; see Supplemental Fig. 3).

The compounds -10 and -15 were examined because of their unique modifications: FAPI-10 is a peptide conjugate of the FAPI-02 core with the intention to localize the radioactivity in the nucleus and

FAPI-15 is similar to FAPI-04 but possesses a triethylene glycol spacer instead of the 1,3-propyl moiety. In both cases the EC_{50}-values were comparable to the parenting radiotracer.

Organ Distribution

To evaluate distribution, tumor uptake and excretion of selected FAPI derivatives biodistribution studies were performed in mice bearing human HT-1080 FAP-expressing xenografts. Fig. 3 shows the results of the biodistribution assays performed with FAPI-04 and -13 compared to the existing data of FAPI-02. FAPI-10 was discarded due to a relative low tumor accumulation 1 and 4 h after administration. Moreover, it was highly accumulated within the kidneys (up to 10 %ID/g; FAPI-02 1.6 %ID/g) with high kidney values even after 24 h (see Supplemental Fig. 5). FAPI-05 produced results comparable to FAPI-02 but was discarded with regard to the better performing derivatives FAPI-04 and -13. Tracer uptake in most normal tissues was slightly higher for FAPI-04 compared to FAPI-02 and further increased for FAPI-13. Tumor accumulation was higher for FAPI-04 and FAPI-13 as compared to FAPI-02, especially after 24 h. A calculation of the area under curve is shown in Supplemental Table 1. The values for FAPI-02, -04 and -15 were 64, 99.4 and 157.5, respectively. However, the tumor-to-blood ratio was in favor of FAPI-04 as compared to FAPI-13 (Supplemental Fig. 6).

Small-Animal PET Imaging

For further characterization of the remaining FAP-inhibitors small-animal PET studies were conducted with HT-1080-FAP xenografted mice (Figs. 4 and 5). Similar to FAPI-02, FAPI-04 demonstrated the highest tumor uptake 1 h after injection with a maximum SUV of 1.2 (FAPI-02: 0.88) which did not significantly decrease within 2 h (SUV 1.1; FAPI-02: 0.71). In contrast, tumor accumulation of FAPI-13 was steadily increasing up to 2 h after injection (SUV 1 h: 0.93; 2 h: 0.97). However, higher background and tracer uptake in spinal cord and bones were observed (Supplemental Fig. 7). Additionally, the xenograft model SK-LMS-1 was also successfully used to demonstrate the applicability of FAPI-04 in a second tumor

entity (Fig. 4). Furthermore, the target specificity was elucidated by a blocking experiment in a HT-1080-FAP-xenograft. As shown in Fig. 5, accumulation in the tumor was suppressed effectively by co-administration of unlabeled compound.

Clinical Application in Patients with Breast Cancer

Diagnostic PET/CT scans were performed 10 min, 1 and 3 hrs after intravenous administration of ^{68}Ga-FAPI-04 in two patients with metastasized breast cancer (Figs. 6 and 7). In both patients a robust accumulation of the tracer was observed in the metastases with maximum SUV values between 7 and 15.5 (patient in Fig. 6) and 15.3 and 29.9 (patient in Fig. 7). In contrast, tracer uptake into normal tissue was very low (Supplemental Table 2). The radioactivity was cleared rapidly from the blood stream and excreted predominantly via the kidneys, resulting in high contrast images. In addition to imaging, therapy with 2.9 GBq ^{90}Y-FAPI-04 was done in one patient. The Bremsstrahlung images showed accumulation of the tracer after 3h and even after 1d p.i. in this patient. This rather low dose led to a significant reduction of pain medication in this case (from baseline morphine and three to four additional morphine administrations per day to baseline medication only).

DISCUSSION

In this work several approaches were investigated to improve the pharmacokinetic properties of the novel quinoline based radiopharmaceuticals developed by our lab (*26*). Herein, a particular focus was on the elaboration of a theranostic tracer, which can be employed for both diagnostics and therapy. This concept is based on the linking of the FAP targeting moiety to the chelator DOTA which allows the incorporation of different isotopes suitable for imaging or therapeutic purposes. Using the ligand FAPI-04 we were able to demonstrate the targeted delivery of the positron emitting Ga-68 as well as the therapeutic nuclide Y-90 in a clinical setting. The main challenge for a potential therapeutic application of the tracer was its optimization regarding tumor uptake and retention time. We addressed this task by

assessing a series of novel compounds based on the initial FAP inhibitor FAPI-02. The most striking improvement is the utilization of 4,4-difluoroproline, which was already successful with respect to enzyme inhibition as described by Jansen *et al*.(*28*). By this substitution the EC_{50} value of FAPI-04 was reduced by a factor of three compared to FAPI-02. Also, the difference of affinity for FAP and DPP4 was shifted in favor of FAPI-04 as shown by FAP/DPP4 binding ratios of 45 and 750 for FAPI-02 and FAPI-04, respectively. In addition, the efflux experiments showed a significantly slower washout of FAPI-04 than FAPI-02, resulting in an increased half-life of 3.0 h (FAPI-02: 1.7 h; Supplemental Fig. 4)

Although FAPI-02 uptake *in vitro* was higher after 1 and 4 h incubation and equal after 24 h, the FAPI-04 PET imaging and biodistribution studies in small animals demonstrated higher accumulation, longer dwell time and no significant increase of background activity. Compared to FAPI-04 FAPI-13 showed higher tumor uptake values leading to a higher area under curve value. However, the retention of the tracer in the blood was higher, leading to lower tumor-to blood values. This may lead to a higher hematotoxicity during treatment, narrowing the therapeutic window. Due to these improvements the therapeutic implementation of ^{90}Y-labeled FAPI-04 was initiated. A stability analysis of FAPI-04 done before in human serum revealed no degradation during 24 hours, qualifying this compound for clinical translation (Supplemental Fig. 1).

A structure-activity relationship analysis was done for modifications of the heterocyclic segment and the position of the linker: The simple 3-amino-1-propyl derivatives FAPI-06 and -07 showed suitable cell-binding at one and four hours but were almost completely eliminated after 24 hours demonstrating that the heterocyclic segment is necessary to enable a sufficiently high retention in the tumor cells. The 7-quinolyl linked compounds FAPI-08 and -09 revealed the same pharmacokinetic profile in the course of incubation which could be explained by the removal of the radiolabeled moiety. This indicates that the position of the linker at the quinoline moiety is equally essential. In FAPI-06 and -07 the bond between DOTA and the propylamine is far more accessible than the piperazine bound DOTA of FAPI-02 and -04, and an enzymatic breakdown can proceed much faster.

The binding to albumin or other plasma proteins with a longer retention time in the circulation is seen as a knock-out criterion for possible theranostics and the reason why FAPI-13 was not considered for further development despite having the lowest EC_{50}-value and the highest tumor accumulation of the compared compounds in tumor-bearing animals. The higher lipophilicity of the piperidine moiety is presumably the cause for higher affinity, better tissue permeation and longer target prevalence, but leads to an unspecific binding to serum proteins, which competes with the attachment to FAP and has a negative impact on the pharmacokinetic properties (*29,30*).

The results of the in vitro as well as the in vivo data led to the clinical transfer of FAPI-04 for the diagnosis and therapy of two patients with metastasized breast cancer. As seen in the animal experiments PET/CT imaging in patients showed a rapid, predominantly renal washout out of the body with an equally rapid accumulation in tumor lesions with SUVs between 7 and 29.9, leading to visualization of metastases even at 10 minutes after tracer administration. Besides this finding, radioactivity was seen only in the renal pelvis and the bladder, with no accumulation in the renal parenchyma and all other organs, making FAPI-04 an attractive tracer for both diagnostic and therapeutic application. In order to fit the physical half-life of the isotope used for therapy to the retention in the tumor, Y-90 with a half-life of 64 h was chosen for treatment. In a proof of principle approach a patient was treated with 2.9 GBq ^{90}Y-FAPI-04 which resulted in visualization of the metastases in Bremsstrahlung images at 24h after tracer administration (Fig. 7). Clinically this was associated with a significant reduction of pain medication. Furthermore, no side effects were observed, especially with respect to hematotoxicity. Since tracer uptake was low in all normal organs we expect that the dose can be significantly increased to obtain tumoricidal effects. However, this has to be done in future approaches based on dosimetric calculations and dose escalation regimens.

CONCLUSION

Based on our previous work on quinoline-based FAP-targeted radiopharmaceuticals, FAPI-04 was successfully developed as a novel theranostic tool. The pharmacokinetic profile of the compound was improved by incorporation of the 4,4-difluoroprolyl building-block. Moreover, a comprehensive analysis of the synthesized compounds provided valuable insights into the structure-activity-relationship of the chelator-carrying side chain.

Of all derivatives tested, FAPI-04 is the most suitable compound for the potential application as a theranostic tracer. Similar to its precursor FAPI-02, it shows a rapid internalization into FAP-positive tumors and a fast clearance from the body resulting in a very fast accumulation at tumor sites (10 minutes after tracer administration) and comparable tumor-to-organ ratios. Moreover, the effective tumor uptake after 24 h is increased by hundred percent in comparison to FAPI-02, which is of great benefit regarding a theranostic application of the tracer. A proof of concept was possible in two patients showing an excellent performance of the tracer for diagnosis and promising first results for therapy. Future development will concentrate on the design of compounds for labeling with other isotopes with different physical characteristics such as ^{188}Re, ^{64}Cu or ^{212}Pb.

ACKNOWLEDGEMENTS

The authors gratefully acknowledge Stefan Bauer (National Center for Tumor Diseases, Heidelberg) for supplying the FAP-α and CD26 transfected cell lines. The authors thank Christian Kleist, Susanne Krämer, Stephanie Biedenstein, Kirsten Kunze, Irina Kupin, Vanessa Kohl, Marlene Tesch, Iris Morr, Sabine Weiss, Christiane Brenner, Karin Leotta and Ursula Schierbaum for excellent technical assistance. This work was funded in part by the Federal Ministry of Education and Research, grant number 13N 13341.

REFERENCES

1. Gascard P, Tlsty TD. Carcinoma-associated fibroblasts: orchestrating the composition of malignancy. *Genes Dev.* 2016;30:1002-1019.

2. Park JE, Lenter MC, Zimmermann RN, Garin-Chesa P, Old LJ, Rettig WJ. Fibroblast activation protein, a dual specificity serine protease expressed in reactive human tumor stromal fibroblasts. *J Biol Chem.* 1999;274:36505-36512.

3. Rettig WJ, Garin-Chesa P, Healey JH, et al. Regulation and heteromeric structure of the fibroblast activation protein in normal and transformed cells of mesenchymal and neuroectodermal origin. *Cancer Res.* 1993;53:3327-3335.

4. Garin-Chesa P, Old LJ, Rettig WJ. Cell surface glycoprotein of reactive stromal fibroblasts as a potential antibody target in human epithelial cancers. *Proc Natl Acad Sci U S A.* 1990;87:7235-7239.

5. Henry LR, Lee HO, Lee JS, et al. Clinical implications of fibroblast activation protein in patients with colon cancer. *Clin Cancer Res.* 2007;13:1736-1741.

6. Cohen SJ, Alpaugh RK, Palazzo I, et al. Fibroblast activation protein and its relationship to clinical outcome in pancreatic adenocarcinoma. *Pancreas.* 2008;37:154-158.

7. Zhang Y, Tang H, Cai J, et al. Ovarian cancer-associated fibroblasts contribute to epithelial ovarian carcinoma metastasis by promoting angiogenesis, lymphangiogenesis and tumor cell invasion. *Cancer Lett.* 2011;303:47-55.

8. Ju MJ, Qiu SJ, Fan J, et al. Peritumoral activated hepatic stellate cells predict poor clinical outcome in hepatocellular carcinoma after curative resection. *Am J Clin Pathol.* 2009;131:498-510.

9. Chen WT, Kelly T. Seprase complexes in cellular invasiveness. *Cancer Metastasis Rev.* 2003;22:259-269.

10. Keane FM, Nadvi NA, Yao TW, Gorrell MD. Neuropeptide Y, B-type natriuretic peptide, substance P and peptide YY are novel substrates of fibroblast activation protein-alpha. *FEBS J.* 2011;278:1316-1332.

11. Huang Y, Wang S, Kelly T. Seprase promotes rapid tumor growth and increased microvessel density in a mouse model of human breast cancer. *Cancer Res.* 2004;64:2712-2716.

12. Kelly T. Fibroblast activation protein-alpha and dipeptidyl peptidase IV (CD26): cell-surface proteases that activate cell signaling and are potential targets for cancer therapy. *Drug Resist Updat.* 2005;8:51-58.

13. Mueller SC, Ghersi G, Akiyama SK, et al. A novel protease-docking function of integrin at invadopodia. *J Biol Chem.* 1999;274:24947-24952.

14. Loeffler M, Kruger JA, Niethammer AG, Reisfeld RA. Targeting tumor-associated fibroblasts improves cancer chemotherapy by increasing intratumoral drug uptake. *J Clin Invest.* 2006;116:1955-1962.

15. Kraman M, Bambrough PJ, Arnold JN, et al. Suppression of antitumor immunity by stromal cells expressing fibroblast activation protein-alpha. *Science.* 2010;330:827-830.

16. Welt S, Divgi CR, Scott AM, et al. Antibody targeting in metastatic colon cancer: a phase I study of monoclonal antibody F19 against a cell-surface protein of reactive tumor stromal fibroblasts. *J Clin Oncol.* 1994;12:1193-1203.

17. Scott AM, Wiseman G, Welt S, et al. A Phase I dose-escalation study of sibrotuzumab in patients with advanced or metastatic fibroblast activation protein-positive cancer. *Clin Cancer Res.* 2003;9:1639-1647.

18. Hofheinz RD, al-Batran SE, Hartmann F, et al. Stromal antigen targeting by a humanised monoclonal antibody: an early phase II trial of sibrotuzumab in patients with metastatic colorectal cancer. *Onkologie.* 2003;26:44-48.

19. Wang LC, Lo A, Scholler J, et al. Targeting fibroblast activation protein in tumor stroma with chimeric antigen receptor T cells can inhibit tumor growth and augment host immunity without severe toxicity. *Cancer Immunol Res.* 2014;2:154-166.

20. Lo A, Wang LC, Scholler J, et al. Tumor-Promoting Desmoplasia Is Disrupted by Depleting FAP-Expressing Stromal Cells. *Cancer Res.* 2015;75:2800-2810.

21. Ostermann E, Garin-Chesa P, Heider KH, et al. Effective immunoconjugate therapy in cancer models targeting a serine protease of tumor fibroblasts. *Clin Cancer Res.* 2008;14:4584-4592.

22. Brennen WN, Rosen DM, Wang H, Isaacs JT, Denmeade SR. Targeting carcinoma-associated fibroblasts within the tumor stroma with a fibroblast activation protein-activated prodrug. *J Natl Cancer Inst.* 2012;104:1320-1334.

23. LeBeau AM, Brennen WN, Aggarwal S, Denmeade SR. Targeting the cancer stroma with a fibroblast activation protein-activated promelittin protoxin. *Mol Cancer Ther.* 2009;8:1378-1386.

24. Lee J, Fassnacht M, Nair S, Boczkowski D, Gilboa E. Tumor immunotherapy targeting fibroblast activation protein, a product expressed in tumor-associated fibroblasts. *Cancer Res.* 2005;65:11156-11163.

25. Teichgraber V, Monasterio C, Chaitanya K, et al. Specific inhibition of fibroblast activation protein (FAP)-alpha prevents tumor progression in vitro. *Adv Med Sci.* 2015;60:264-272.

26. Loktev A, Lindner T, Mier W, et al. A New Method for Tumor Imaging by Targeting Cancer Associated Fibroblasts. *J Nucl Med.* 2018;in press.

27. Fischer E, Chaitanya K, Wuest T, et al. Radioimmunotherapy of fibroblast activation protein positive tumors by rapidly internalizing antibodies. *Clin Cancer Res.* 2012;18:6208-6218.

28. Jansen K, Heirbaut L, Verkerk R, et al. Extended Structure–Activity Relationship and Pharmacokinetic Investigation of (4-Quinolinoyl)glycyl-2-cyanopyrrolidine Inhibitors of Fibroblast Activation Protein (FAP). *Journal of Medicinal Chemistry.* 2014;57:3053-3074.

29. Meanwell NA. Improving Drug Candidates by Design: A Focus on Physicochemical Properties As a Means of Improving Compound Disposition and Safety. *Chemical Research in Toxicology.* 2011;24:1420-1456.

30. Testa B, Crivori P, Reist M, Carrupt P-A. The influence of lipophilicity on the pharmacokinetic behavior of drugs: Concepts and examples. *Perspectives in Drug Discovery and Design.* 2000;19:179-211.

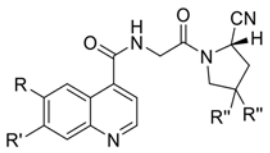

Name	R	R´	R´´	EC_{50} [nM]
FAPI-02§	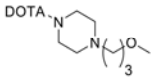	H	H	21
FAPI-03	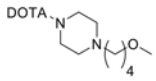	H	H	n.d.
FAPI-04	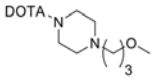	H	F	6.5
FAPI-05	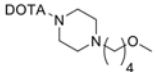	H	F	17
FAPI-06	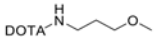	H	H	n.d.
FAPI-07	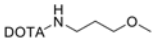	H	F	n.d.
FAPI-08	H	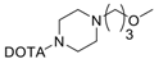	H	n.d.
FAPI-09	H	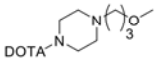	F	n.d.
FAPI-10	H-PAAKRVKLDK*C**-OH	H	H	21
FAPI-11	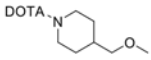	H	F	n.d.
FAPI-12	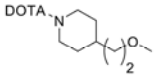	H	F	n.d.
FAPI-13	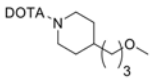	H	F	4.5
FAPI-14	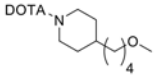	H	F	n.d.
FAPI-15	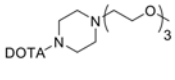	H	F	9.1

FIGURE 1. Overview of the synthesized FAPI derivatives. EC_{50} values obtained by competition experiments are shown for selected compounds. §discussed in previous publication (*28*). *ε-amine modified by DOTA. **cysteine-thiol attached to a maleimide carrying piperazinylpropoxy moiety.

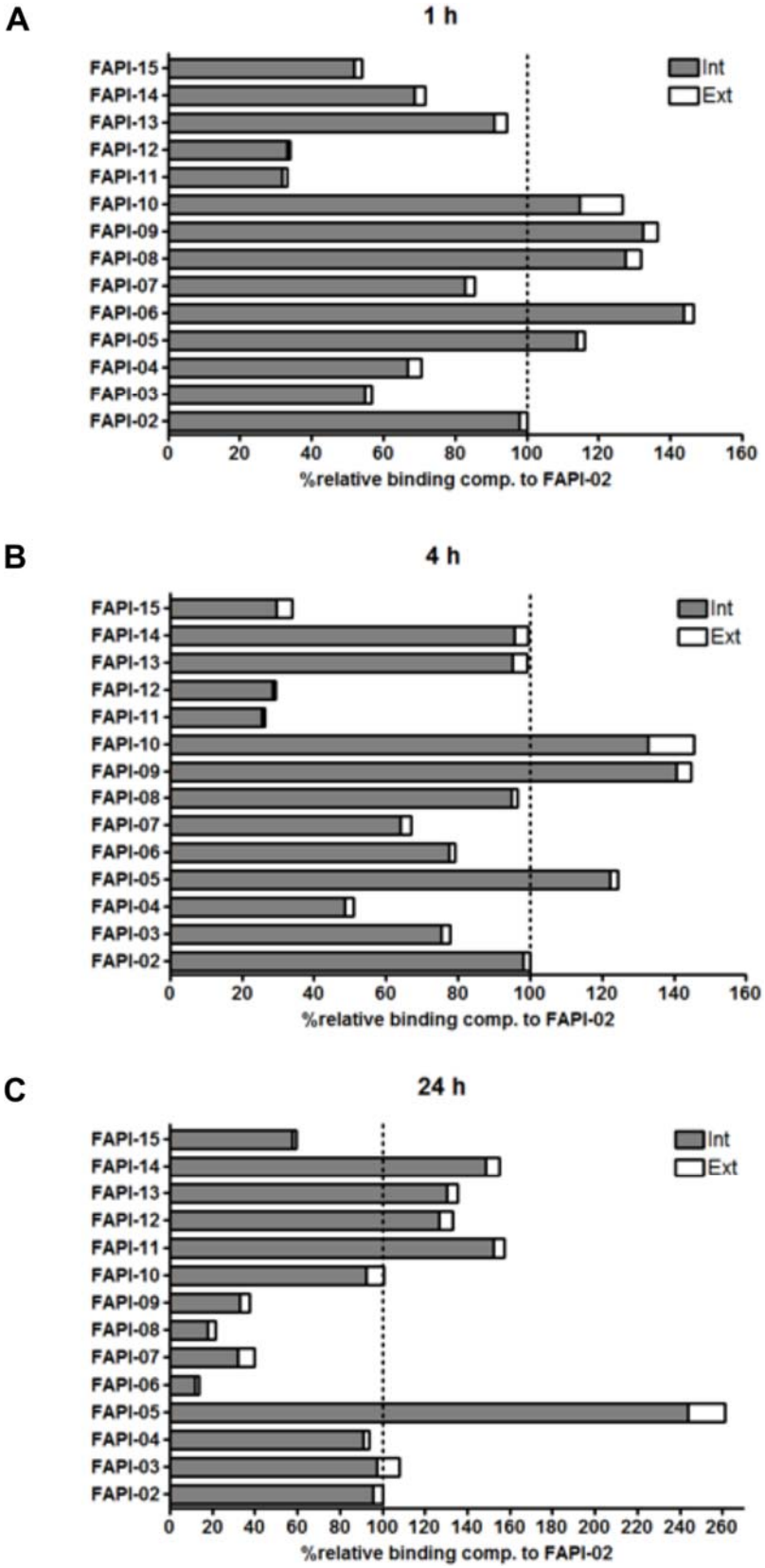

FIGURE 2. Relative binding and internalization rates of ^{177}Lu-labeled FAPI derivatives compared to FAPI-02 (set to 100%) on FAP-expressing HT-1080 cells.

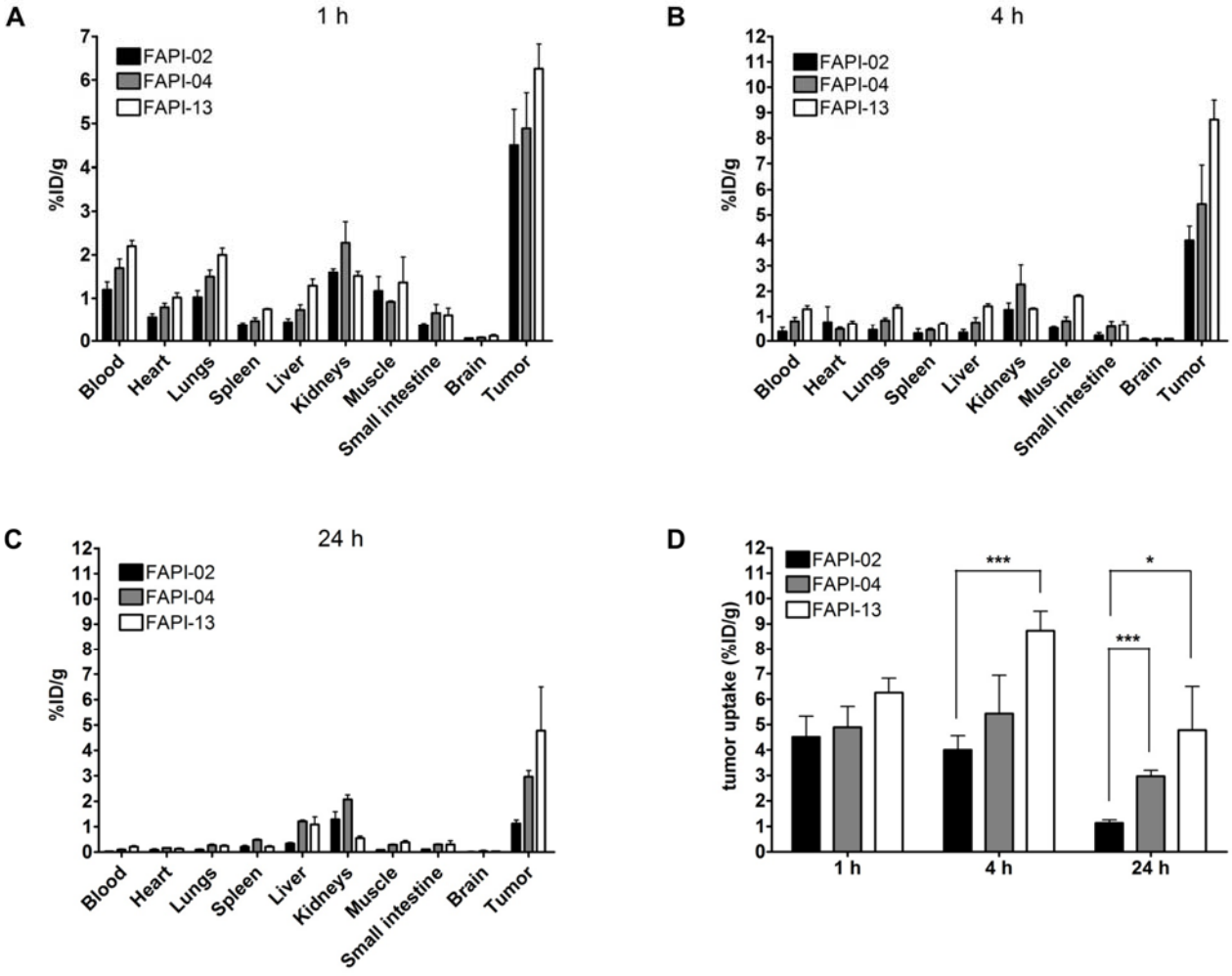

FIGURE 3. Biodistribution of selected FAPI derivatives in HT-1080-FAP xenotransplants 1 (A), 4 (B) and 24 h (C) after intravenous administration of the radiotracers. D. Tumor uptake of the selected compounds.

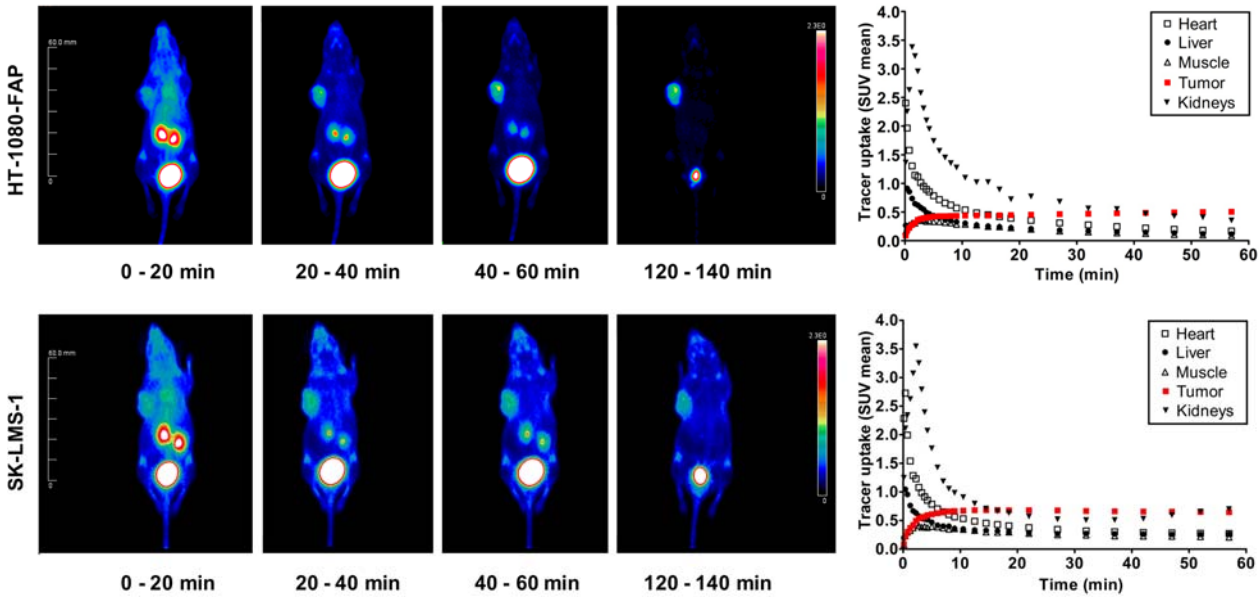

FIGURE 4. PET imaging of FAPI-04 in mice bearing SK-LMS-1 and HT-1080-FAP tumors

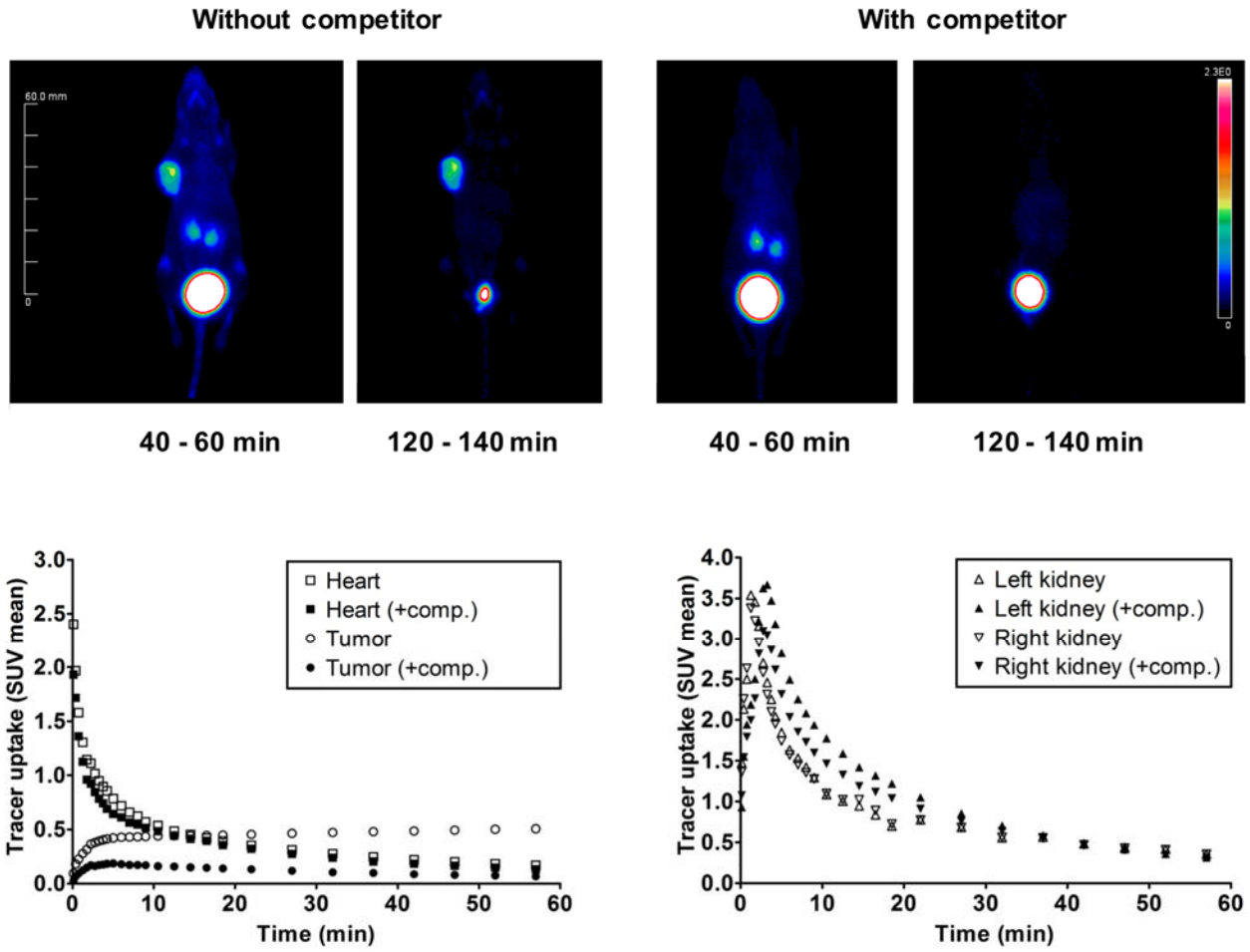

FIGURE 5. PET imaging of FAPI-04 in HT-1080-FAP tumor bearing mice with and without simultaneous injection of unlabeled FAPI-04 as competitor.

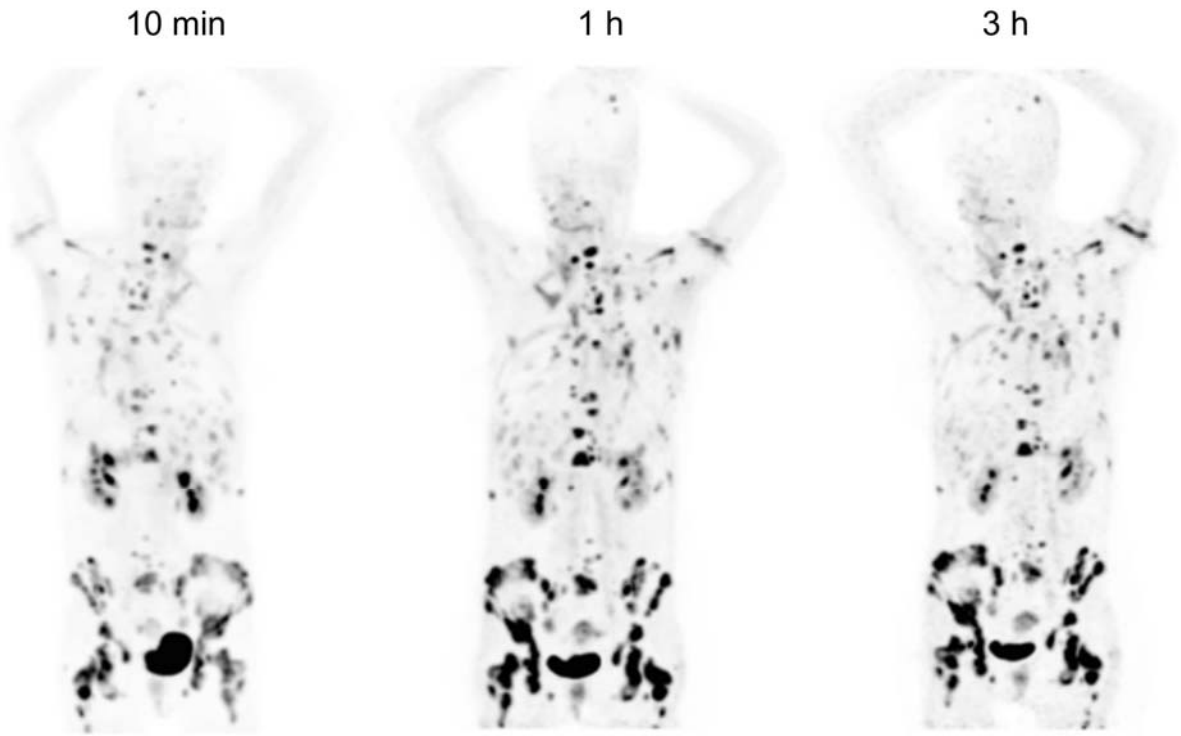

FIGURE 6. Maximum intensity projections (MIP) of PET/CT scans in a patient with metastasized breast cancer at 10 min, 1 h and 3 h after intravenous administration of 263 MBq ^{68}Ga-FAPI-04. The images revealed activity in the renal pelvis, the bladder and in the metastases. Normal organs showed a very low uptake resulting in a very high image contrast.

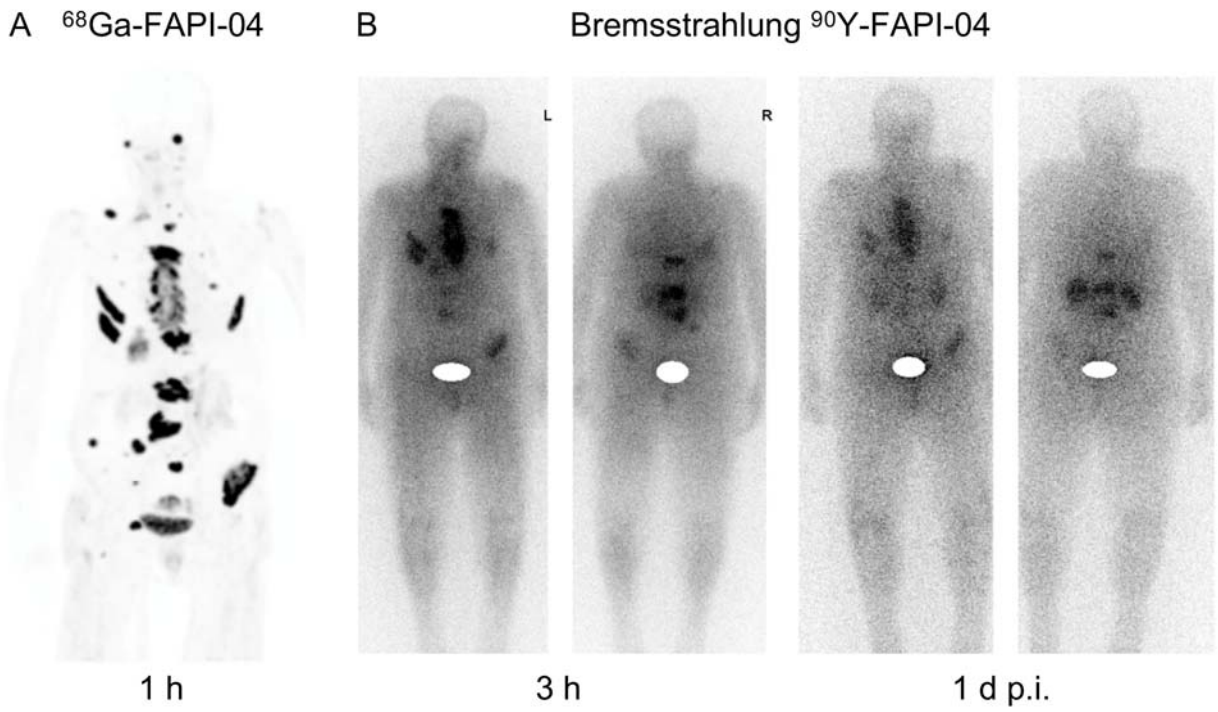

FIGURE 7. A. Maximum intensity projection (MIP) 1 h after intravenous administration of 270 MBq ^{68}Ga-FAPI-04 to one patient with metastasized breast cancer. B. Imaging of Bremsstrahlung 3 h and 1 day after therapeutic treatment with ^{90}Y-FAPI-04 of the same patient.

GENERAL INFORMATIONS

REAGENTS

All solvents and non-radioactive reagents (except for solid phase peptide synthesis) were obtained in reagent grade from ABCR (Karlsruhe, Germany), Sigma-Aldrich (München, Germany), Acros Organics (Geel, Belgium) or VWR (Bruchsal, Germany) and were used without further purification. The intermediates 6-methoxyquinoline-4-carboxylic acid, 7-methoxyquinoline-4-carboxylic acid, 5-bromoquinoline-4-carboxylic acid and (*S*)-1-(2-aminoacetyl)pyrrolidine-2-carbonitrile 4-methylbenzenesulfonate were synthesized following the protocols of Jansen *et al*. (*1,2*) and Loktev *et al.* (*3*). The substance (*S*)-*N*-(2-(2-cyanopyrrolidin-1-yl)-2-oxoethyl)-5-bromoquinoline caboxamide was synthesized by the general amidation protocol. FAPI-02 and its intermediates were synthesized according to (*3*). The substance (*S*)-1-(2-aminoacetyl)-4,4-difluoropyrrolidine-2-carbonitrile 4-methylbenzene-sulfonate was synthesized following Jansen *et al*. (*2*). 4-alkyl-piperidine mesylates were synthesized from the corresponding amino alcohols by *N*-Boc protection and *O*-mesylation following standard procedures (e.g. (*4*)). 2,2',2''-(10-(2-(4-nitrophenyl)oxy)-2-oxoethyl)-1,4,7,10-tetraazacyclododecane-1,4,7triyl)triacetic acid (DOTA-PNP) was synthesized following the protocol of Mier *et al.* (*5*). Radioactive lutetium (^{177}Lu) was obtained from ITG (München, Germany); radioactive gallium (^{68}Ga) was eluted from a ^{68}Ge-/^{68}Ga generator.

PEPTIDE SYNTHESIS

SPPS was conducted on a fully automated peptide synthesizer (Applied Biosystems 433A, Carlsbad, CA, USA). Fmoc-deprotection efficiency was monitored at 301 nm. Solvents, piperidine, HBTU and DIPEA were obtained from Biosolve (Valkenswaard, Netherlands) PS AM Rink amide resin (substitution level: 0.74 mmol/g; Iris-Biotech, Marktredwitz, Germany) was used with 5 equivalents of dedicated 9-fluorenylmethoxycarbonyl (Fmoc)-protected L-α-amino acid building blocks (Orpegen, Heidelberg, Germany). Fmoc-Lys(Alloc)-OH (Iris-Biotech, Marktredwitz, Germany) was used for the side chain attachment of tris-tBu-DOTA.

The synthesis cycle consisted of: i) Fmoc cleavage: 20% piperidine/NMP, ii) NMP washings, iii) coupling: Fmoc-AA-OH/HBTU/DIPEA/peptidyl-resin 5/4.5/10/1, 8 min, iv) NMP washings.

Alloc-deprotection was achieved by incubating the resin with a solution of 5 mg tetrakistriphenylphosphinepalladium(0) and 20 mg borane dimethylamino complex in 2 mL dichloromethane for 20 min. The resin is washed thoroughly before the resin was incubated with 2 eq. HATU-preactivated tris-tBu-DOTA.

Cleavage from the solid support was performed with 95:5:2.5:2.5 TFA/ethanedithiol/water/triisopropylsilane for over 6 h at ambient temperature and the peptide was subsequently precipitated with cold diethyl ether. The precipitate was separated by centrifugation (3300 rpm, 5 min) washed with diethyl ether, dried and purified by HPLC.

HIGH PERFORMANCE LIQUID CHROMATOGRAPHY

Reverse-phase high-performance liquid chromatography (RP-HPLC) was conducted using linear gradients (0-100% acetonitrile in 5 min; flowrate 2 mL/min) of 0.1% TFA in water and in acetonitrile on a Chromolith Performance RP-18e column (100 × 3 mm; Merck KGaA Darmstadt, Germany). UV-absorbance was detected at 214 nm. An additional γ-detector was used for the HPLC-analysis of radioactive compounds. HPLC-MS characterization was performed on an ESI mass spectrometer (Exactive, Thermo Fisher Scientific, Waltham, MA, USA) connected to an Agilent 1200 HPLC system with a Hypersil Gold C18 1.9 µm column (200 × 2.1 mm; 0-100% acetonitrile in 20 min; flowrate 200 µL/min). Analytical radio-HPLC was performed using a Chromolith Performance RP-18e column (100×3mm; Merck; 0-30% acetonitrile in 10 min; flowrate 2 mL/min); the same conditions were applied for the determination of serum stability. HPLC-purifications were performed on a LaPrep P110-System (Knauer, Berlin, Germany) and a Reprosil Pur 120 column (C18-aq 5 µm 250 × 25mm; Dr. Maisch, Ammerbuch-Entringen, Germany). The gradient (15 or 25 min; flowrate 20 mL/min) was modified for the individual products.

SYNTHESIS

The principle synthesis strategy of the FAPI derivatives is shown for FAPI-04 (Supplemental Fig. 1). First demethylation of 6-hydroxyquinolie-4-carboxylic acid was performed, followed by etherification with excess 1-bromo-3-chloropropane. Next an amination was conducted with 1-*tert*-butoxycarbonylpiperazine in the presence of potassium iodide as catalyst. Afterwards the carboxylic acid was coupled to the glycyl-prolyl building block **1**. Finally, the Boc-group was removed and the amine acylated by DOTA-PNP after neutralization. The nuclear localization signal peptide of c-Myc was conjugated to FAPI-02 via Michael addition. For this purpose an auxiliary cysteine residue in the peptide was coupled to a maleimido group which was attached at the available piperazine-amine.

For the compounds FAPI-06 and -07 a Staudinger reductive amination followed by Boc-protection was applied instead of the substitution with *N*-Boc-piperazine. For FAPI-11 to -14 the *N*-Boc-4-alkylpiperidine function was attached during the etherification step. In case of FAPI-15 8-(1-Boc-piperazin-4-yl)triethyleneglycol-1-*p*-toluene sulfonate was used.

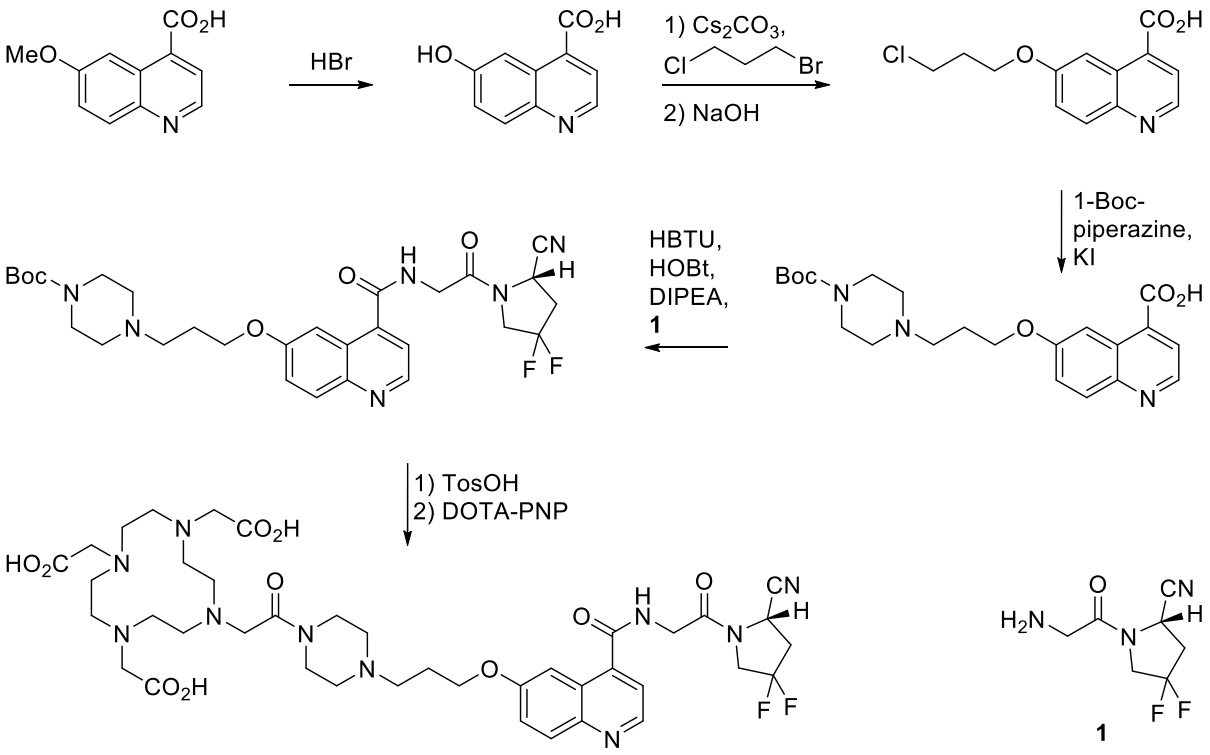

SUPPLEMENTAL FIGURE 1. Synthetic pathway towards FAPI-04.

General 6-OH alkylation protocol A

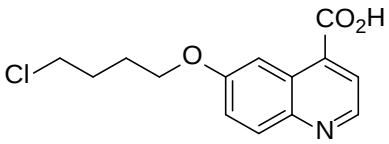

6-(4-chlorobutoxy)quinoline-4-carboxylic acid

20.2 µL (30.1 mg; 176 µmol) 1-bromo-4-chlorobutane were added to a suspension of 9.52 mg (50.3 µmol) 6-hydroxyquinoline-4-carboxylic acid and 159 mg (489 µmol) caesium carbonate in 250 µL DMF and heated to 60 °C over night. The reation mixture was cooled to room temperature, diluted with 250 µL water and 500 µL acetonitrile before 100 µL 6 M NaOH were added. The reaction mixture was directly purified via HPLC (5-40%) after the complete ester hydrolysis was accomplished. 10.1 mg (35.8 µmol; 71%) of the product were obtained after lyophilization.

^{1}H NMR (500 MHz, DMSO-d6) 13.76 (br, 0.5H), 8.86 (d, J = 4.4 Hz, 1H), 8.17 (d, J = 2.4 Hz, 1H), 8.02 (d, J = 9.4 Hz, 1H), 7.92 (d, J = 4.4 Hz, 1H), 7.50 (dd, J = 9.4, 2.4 Hz, 1H), 4.16 (br s, 2H), 3.74 (br s, 2H), 1.94 (br s, 4H); **^{13}C NMR** (125 MHz, DMSO-d6) 167.6, 157.6, 147.5, 144.7, 133.8, 131.2, 125.9, 122.6, 122.2, 104.5, 67.1, 45.2, 28.9, 26.1; **LC-MS** R_t 12.62 min, m/z 280.0590 $[M+H]^+$

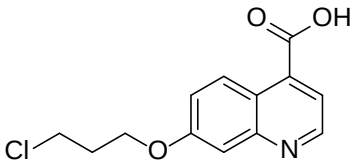

7-(3-chloropropoxy)quinoline-4-carboxylic acid

14.87 mg (55.9 µmol; 56%) were obtained following the general 6-OH alkylation protocol A.

^{1}H NMR (500 MHz, DMSO-d6) 13.79 (br, 0.4H), 8.97 (d, J = 4.5 Hz, 1H), 8.63 (d, J = 9.4 Hz, 1H), 7.79 (d, J = 4.5 Hz, 1H), 7.51 (d, J = 2.2 Hz, 1H), 7.41 (dd, J = 9.4, 2.2 Hz, 1H), 4.30 (t, J = 6.0 Hz, 2H), 3.85 (t, J = 6.5 Hz, 2H), 2.27 (m, 2H); **^{13}C NMR** (125 MHz, DMSO-d6) 167.5, 159.2, 150.4, 150.0, 136.0, 126.9, 120.9, 119.8, 119.6, 108.2, 64.7, 41.9, 31.5; **LC-MS** R_t 10.76 min, m/z 266.0440 $[M+H]^+$

Amination

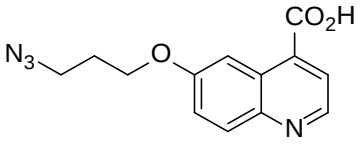

6-(3-azidopropoxy)quinoline-4-carboxylic acid

3.29 mg (12.4 µmol) 6-(3-chloropropoxy)quinoline-4-carboxylic acid, 10.5 mg (160 µmol) sodium azide and 21.0 mg (126 µmol) potassium iodide were suspended in 300 µL dimethylformamide and heated to 60 °C for 20 hours. 2.87 mg (10.6 µmol; 85%) of the title compound were obtained after HPLC purification and freeze-drying.

LC-MS R_t 11.28 min, m/z 295.0649 $[M+Na]^+$

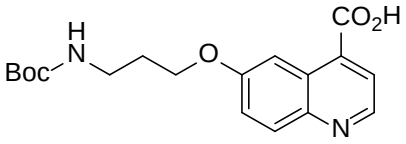

6-(3-(*tert*-butoxycarbonylamino)propoxy)quinoline-4-carboxylic acid

12.3 µL (10.1 mg; 49.9 µmol) tributylphosphine were added to a solution of 1.93 mg (7.10 µmol) 6-(3-azidopropoxy)quinoline-4-carboxylic acid in 270 µL dimethylformamide and 30 µL water. After 5 hours 15.8 mg (72.5 µmol) di-*tert*-butyl dicarbonate and 20.0 µL (14.6 mg; 145 µmol) triethylamine were added. After 1 hour the mixture was purified by HPLC. 1.25 mg (3.62 µmol; 51%) of the title compound were obtained after freeze-drying.

LC-MS R_t 9.53 min, m/z 369.1292 $[M+Na]^+$

General 4-Boc-piperazine attachment

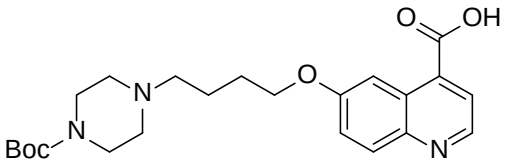

6-(4-(4-*tert*-butoxycarbonylpiperazin-1-yl)butoxy)quinoline-4-carboxylic acid

10.3 mg (36.7 µmol) of 6-(4-chlorobutoxy)quinoline-4-carboxylic acid, 39.2 mg (210 µmol) *N*-*tert*-butoxycarbonylpiperazine and 37.4 mg (226 µmol) potassium iodide were dissolved in 250 µL DMF. The reaction was shaken at 60 °C over night. The resulting suspension was diluted with 750 µL water before the product was purified by HPLC. After freeze drying 17.7 mg (32.5 µmol; 89%) of the product were obtained as the corresponding TFA-salt.

^{1}H NMR (500 MHz, D_2O) 8.92 (d, J = 5.7 Hz, 1H), 8.16 (d, J = 9.3 Hz, 1H), 7.93 (d, J = 5.7 Hz, 1H), 7.80 (dd, J = 9.3, 2,3 Hz, 1H), 7.65 (d, J = 2.3 Hz, 1H), 4.32-4.20 (m, 4H), 3.60 (d, J = 11.8 Hz), 3.32-3.20 (m, 4 H), 3.15-3.03 (m, 2H), 1.98 (br s, 4H), 1.47 (s, 9H); **^{13}C NMR** (125 MHz, D_2O) 159.1, 155.5, 155.4, 141.4, 141.2, 134.5, 134.4, 128.1, 126.7, 122.2, 118.3, 105.2, 82.8, 68.0, 56.5, 51.5, 51.3, 27.4, 25.2, 20.3; **LC-MS** R_t 10.88 min, m/z 430.2115 $[M+H]^+$

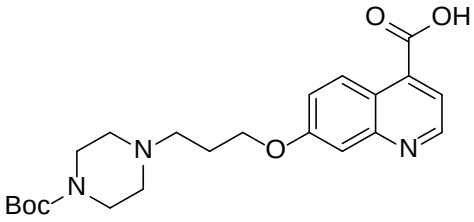

7-(3-(4-*tert*-butoxycarbonylpiperazin-1-yl)propoxy)quinoline-4-carboxylic acid

11.83 mg (28.5 µmol; 84%) were obtained following the previous protocol.

LC-MS R_t 10.37 min, m/z 416.1994 $[M+H]^+$

General 6-OH alkylation protocol B

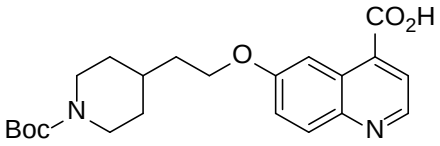

6-(2-(4-*tert*-butoxycarbonylpiperidin-1-yl)ethoxy)quinoline-4-carboxylic acid

A mixture of 3.46 mg (18.3 µmol) 6-hydroxyquinoline-4-carboxylic acid, 62.38 mg (191 µmol) cesium carbonate, 27.3 mg (164 µmol) potassium iodide and 21.25 mg (69.2 µmol) *N*-Boc-4-(2-(metylsulfonyl)oxy)-1-ethylpiperidine in 250 µL DMF and 500 µL acetonitrile were heated to 60 °C over night. The mixture was further diluted with 500 µL water/acetonitrile 1:1 and purified by HPLC. 4.29 mg (10.7 µmol; 59%) of the product were obtained after freeze drying.

LC-MS R_t 15.52 min, m/z 423.1673 $[M+Na]^+$

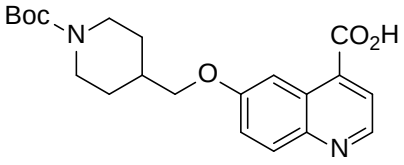

6-((4-*tert*-butoxycarbonylpiperidin-1-yl)methoxy)quinoline-4-carboxylic acid

6.31 mg (16.3 µmol; 98%) were obtained from 6-hydroxyquinoline-4-carboxylic acid and *N*-Boc-4-bromomethylpiperidine following General 6-OH alkylation protocol B.

LC-MS R_t 14.85 min, m/z 409.1521 $[M+Na]^+$

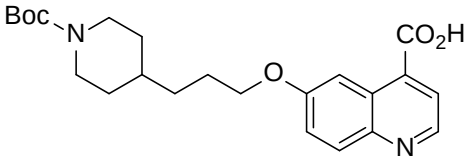

6-(3-(4-*tert*-butoxycarbonylpiperidin-1-yl)propoxy)quinoline-4-carboxylic acid

6.90 mg (16.6 µmol; 82%) were obtained following General 6-OH alkylation protocol B.

LC-MS R_t 16.28 min, m/z 437.1860 $[M+Na]^+$

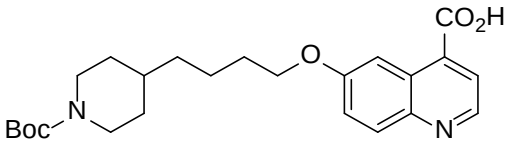

6-(4-(4-*tert*-butoxycarbonylpiperidin-1-yl)butoxy)quinoline-4-carboxylic acid

7.20 mg (16.8 µmol; 84%) were obtained following general 6-OH alkylation protocol B.

LC-MS R_t 17.23 min, m/z 451.1970 $[M+Na]^+$

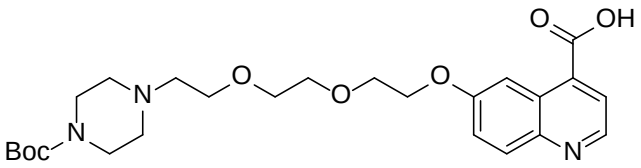

6-(2-(2-(2-(4-*tert*-butoxycarbonylpiperazin-1-yl)ethoxy)ethoxy)ethoxy)quinoline-4-carboxylic acid

9.64 mg (19.7 µmol; 80%) were obtained following general 6-OH alkylation protocol B.

LC-MS R_t 10.90 min, m/z 490.2327 $[M+H]^+$

General amidation protocol

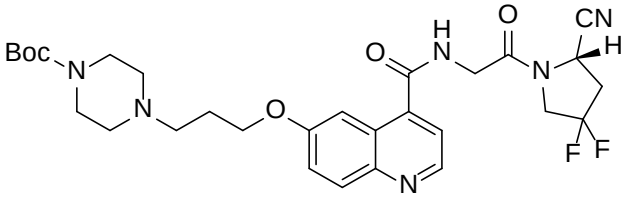

(*S*)-*N*-(2-(2-cyano-4,4-difluoropyrrolidin-1-yl)-2-oxoethyl)-6-(3-(4-*tert*-butoxycarbonylpiperazin-1-yl)propoxy)quinoline-4-carboxamide

13.3 mg (35.0 µmol) HBTU in 100 µL DMF were added to a solution of 12.5 mg (30.0 µmol) 6-(3-(4-*tert*-butoxycarbonylpiperazin-1-yl)-1-propoxy)quinoline-4-carboxylic acid, 7.87 mg (58.3 µmol) HOBt and 13.7 µL (10.1 mg; 75 µmol) DIPEA in 100 µL DMF. After 15 min 17.3 mg (37.5 µmol) (*S*)-1-(2-aminoacetyl)-4,4-difluoropyrrolidine-2-carbonitrile 4-methylbenzenesulfonate and 13.7 µL (10.1 mg; 75 µmol) DIPEA in 100 µL DMF were added. The reaction was quenched with 850 µL water and purified by HPLC. Freeze drying provides 13.2 mg (22.4 µmol; 75%) of the title compound.

LC-MS R_t 11.84 min, m/z 605.2610 $[M+Na]^+$

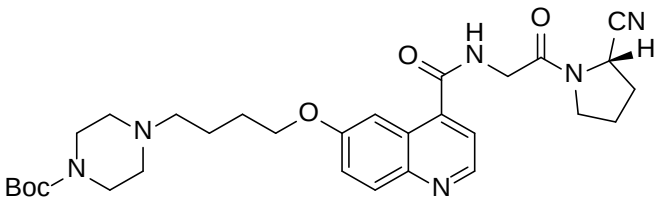

(*S*)-*N*-(2-(2-cyanopyrrolidin-1-yl)-2-oxoethyl)-6-(4-(4-*tert*-butoxycarbonylpiperazin-1-yl)butoxy)quinoline-4-carboxamide

1.49 mg (2.64 µmol; 79%) were obtained following the general amidation protocol.

LC-MS R_t 9.52 min, m/z 565.2937 $[M+H]^+$

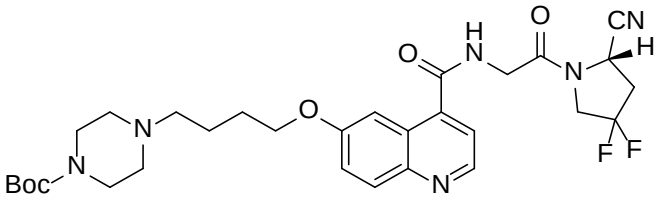

(*S*)-*N*-(2-(2-cyano-4,4-difluoropyrrolidin-1-yl)-2-oxoethyl)-6-(4-(4-*tert*-butoxycarbonylpiperazin-1-yl)butoxy)quinoline-4-carboxamide

4.12 mg (6.86 µmol; 55%) were obtained following the general amidation protocol.

LC-MS R_t 9.74 min, m/z 601.2735 $[M+H]^+$

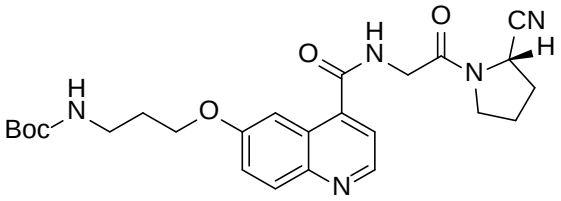

(*S*)-*N*-(2-(2-cyanopyrrolidin-1-yl)-2-oxoethyl)-6-(3-*tert*-butoxycarbonylaminopropoxy)quinoline-4-carboxamide

1.33 mg (2.75 µmol; 66%) were obtained following the general amidation protocol.

LC-MS R_t 10.49 min, m/z 504.2034 $[M+Na]^+$

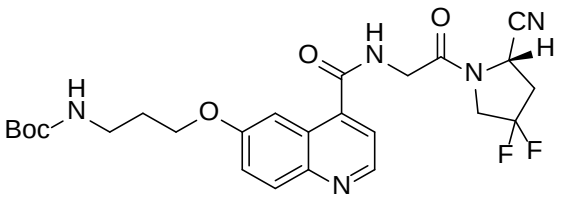

(*S*)-*N*-(2-(2-cyano-4,4-difluoropyrrolidin-1-yl)-2-oxoethyl)-6-(3-*tert*-butoxycarbonylaminopropoxy)quinoline-4-carboxamide

1.56 mg (3.02 µmol; 71%) were obtained following the general amidation protocol.

LC-MS R_t 10.72 min, m/z 540.1835 $[M+Na]^+$

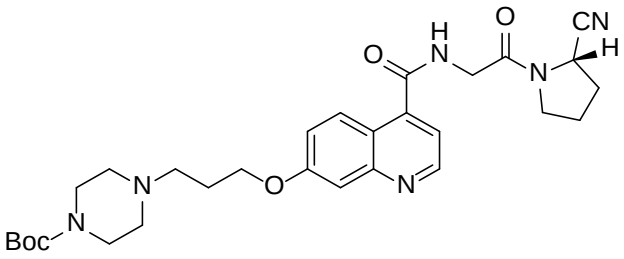

(*S*)-*N*-(2-(2-cyanopyrrolidin-1-yl)-2-oxoethyl)-7-(3-(4-*tert*-butoxycarbonylpiperazin-1-yl)propoxy)quinoline-4-carboxamide

1.63 mg (2.96 µmol; 63%) were obtained following the general amidation protocol.

LC-MS R_t 8.92 min, m/z 573.2581 $[M+Na]^+$

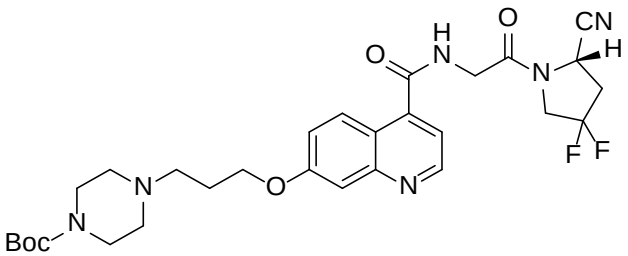

(*S*)-*N*-(2-(2-cyano-4,4-difluoropyrrolidin-1-yl)-2-oxoethyl)-7-(3-(4-*tert*-butoxycarbonylpiperazin-1-yl)-1-propoxy)quinoline-4-carboxamide

2.47 mg (4.21 µmol; 50%) were obtained following the general amidation protocol.

LC-MS R_t 8.96 min, m/z 609.2379 $[M+Na]^+$

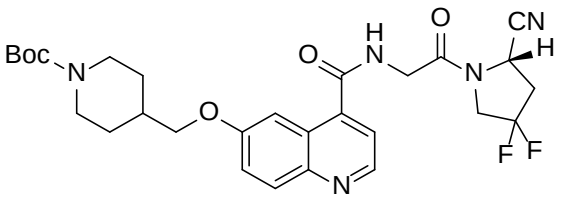

(*S*)-*N*-(2-(2-cyano-4,4-difluoropyrrolidin-1-yl)-2-oxoethyl)-6-((4-*tert*-butoxycarbonylpiperidin-1-yl)methoxy)quinoline-4-carboxamide

2.95 mg (5.29 µmol; 83%) were obtained following the general amidation protocol.

LC-MS R_t 11.33 min, m/z 580.2089 $[M+Na]^+$

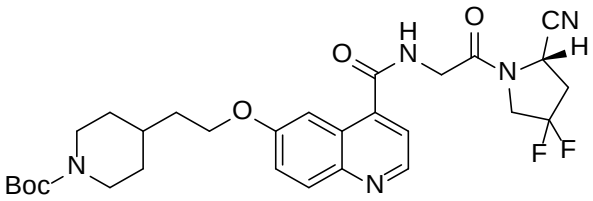

(*S*)-*N*-(2-(2-cyano-4,4-difluoropyrrolidin-1-yl)-2-oxoethyl)-6-(3-(4-*tert*-butoxycarbonylpiperidin-1-yl)-1-ethoxy)quinoline-4-carboxamide

2.82 mg (4.93 µmol; 81%) were obtained following the general amidation protocol.

LC-MS R_t 11.79 min, m/z 594.2241 $[M+Na]^+$

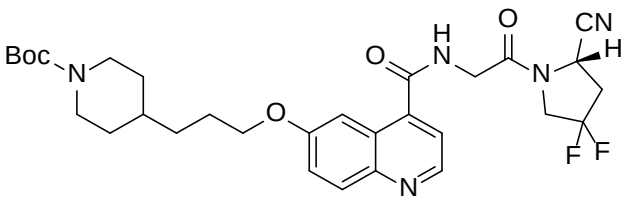

(*S*)-*N*-(2-(2-cyano-4,4-difluoropyrrolidin-1-yl)-2-oxoethyl)-6-(3-(4-*tert*-butoxycarbonylpiperidin-1-yl)-1-propoxy)quinoline-4-carboxamide

2.45 mg (4.46 µmol; 63%) were obtained following the general amidation protocol.

LC-MS R_t 16.73 min, m/z 608.2343 $[M+Na]^+$

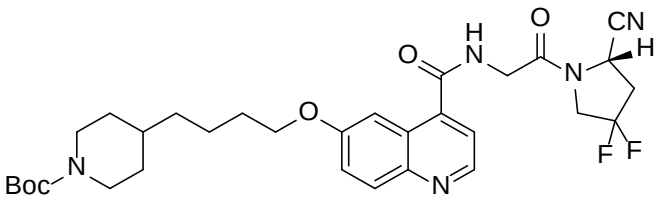

(*S*)-*N*-(2-(2-cyano-4,4-difluoropyrrolidin-1-yl)-2-oxoethyl)-6-(3-(4-*tert*-butoxycarbonylpiperidin-1-yl)-1-butoxy)quinoline-4-carboxamide

3.07 mg (5.45 µmol; 77%) were obtained following the general amidation protocol.

LC-MS R_t 17.34 min, m/z 600.2682 $[M+H]^+$

General modification with actived esters

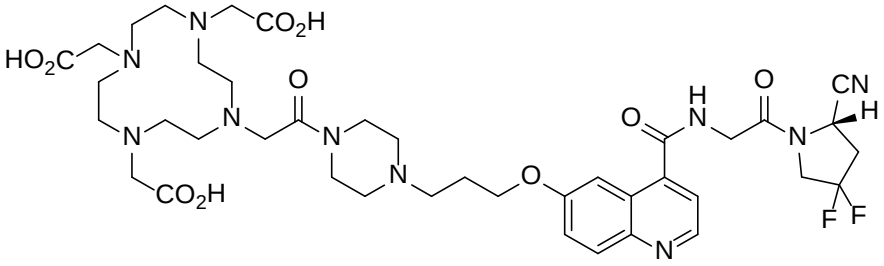

FAPI-04

3.11 mg (8.04 µmol) (*S*)-*N*-(2-(2-cyano-4,4-difluoropyrrolidin-1-yl)-2-oxoethyl)-6-(3-(4-*tert*-butoxycarbonyl-piperazin-1-yl)-1-propoxy)quinoline-4-carboxamide were dissolved in 400 µL acetonitrile and 9.51 mg (49.8 µmol) 4-methylbenzenesulfonic acid monohydrate were added. The reaction was shaken at 45 °C for 2 h, before volatiles were removed under reduced pressure. The residue was taken up in 150 µL dimethylformamide and 25.0 µL (18.25 mg; 181 µmol) triethylamine before 4.50 mg (8.57 µmol) of DOTA-*p*-nitrophenol ester were added. The reaction mixture was diluted with 0.7 mL water and purified by HPLC after shaking for two hours. 3.97 mg (4.55 µmol; 57%) were obtained after freeze drying.

LC-MS R_t 8.80 min, m/z 873.3664 $[M+H]^+$

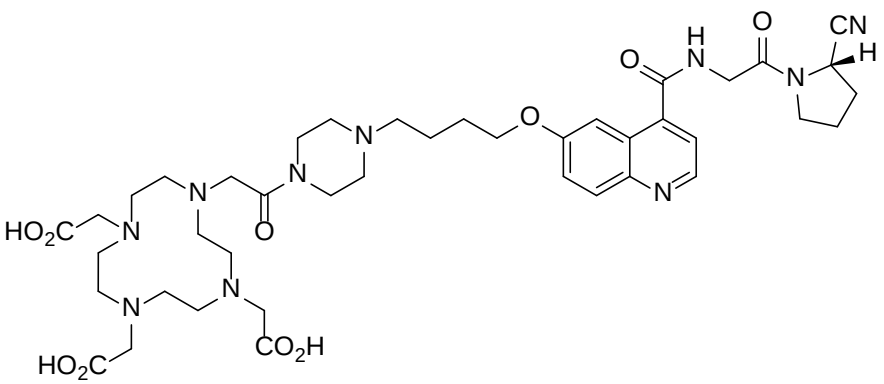

FAPI-03

1.06 mg (1.25 µmol; 69%) were obtained following the general active ester modification protocol.

LC-MS R_t 8.62 min, m/z 851.4017 $[M+H]^+$

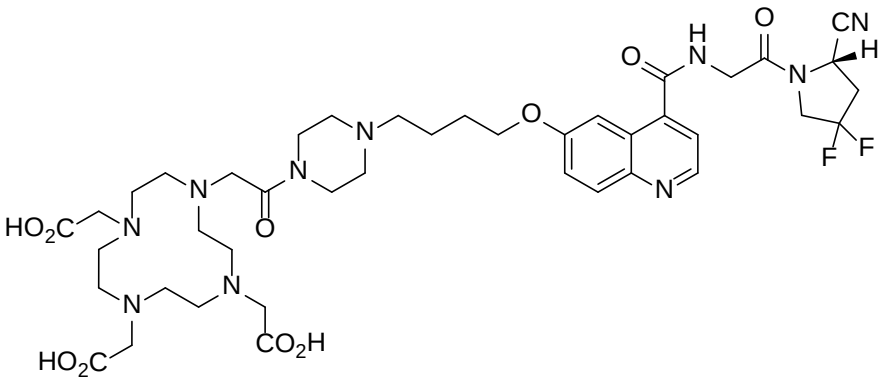

FAPI-05

1.32 mg (1.49 µmol; 76%) were obtained following the general active ester modification protocol.

LC-MS R_t 9.12 min, m/z 887.3814 $[M+H]^+$

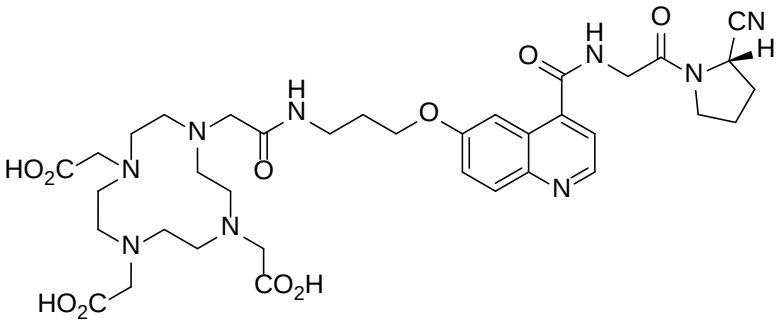

FAPI-06

1.84 mg (2.40 µmol; 81%) were obtained following the general active ester modification protocol.

LC-MS R_t 8.72 min, m/z 768.3328 $[M+H]^+$

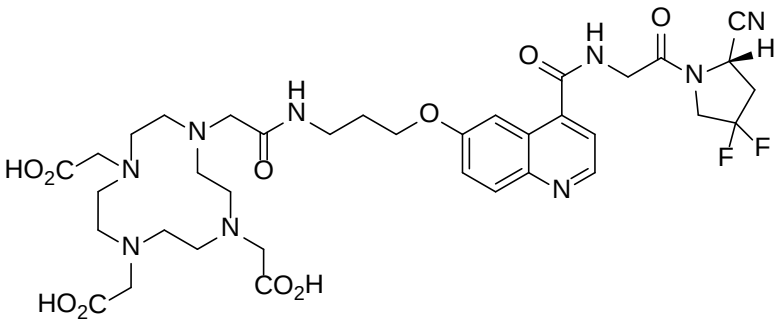

FAPI-07

2.14 mg (2.66 µmol; 88%) were obtained following the general active ester modification protocol.

LC-MS R_t 9.24 min, m/z 804.3121 $[M+H]^+$

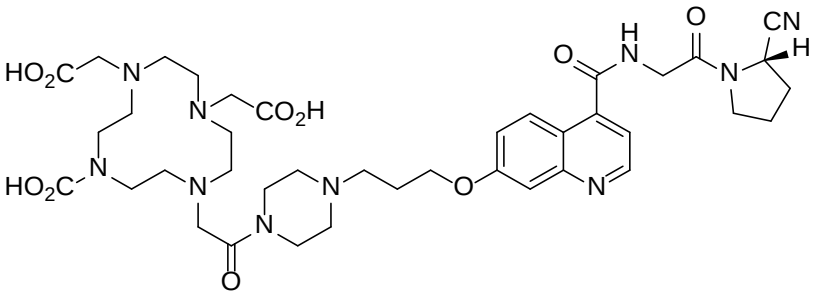

FAPI-08

0.42 mg (0.51 µmol; 32%) were obtained following the general active ester modification protocol.

LC-MS R_t 8.45 min, m/z 837.3870 $[M+H]^+$

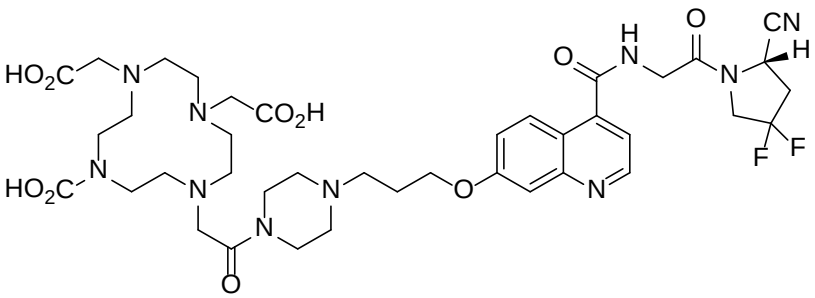

FAPI-09

1.10 mg (1.26 µmol; 78%) were obtained following the general active ester modification protocol.

LC-MS R_t 9.08 min, m/z 873.3664 $[M+H]^+$

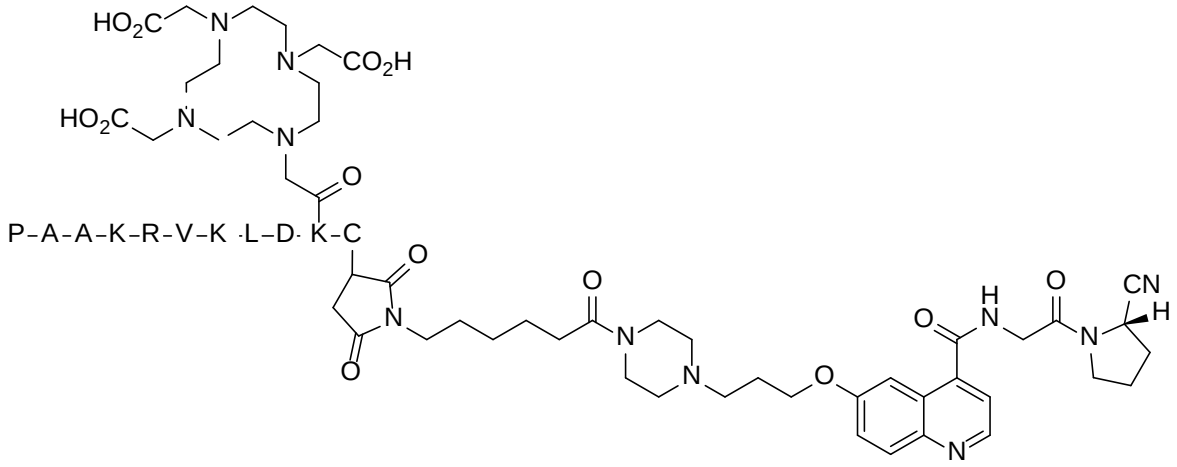

FAPI-10

1.06 mg (1.92 µmol) (*S*)-*N*-(2-(2-cyanopyrrolidin-1-yl)-2-oxoethyl)-6-(3-(4-*tert*-butoxycarbonyl-piperazin-1-yl)-1-propoxy)quinoline-4-carboxamide were dissolved in 200 µL acetonitrile and 4.31 mg (22.6 µmol) 4-methylbenzenesulfonic acid monohydrate were added. The reaction was shaken at 45 °C for 2 h, before volatiles were removed under reduced pressure. Meanwhile 0.80 mg (2.11 µmol) HBTU in 50 µL DMF were added to 0.41 mg (1.92 µmol) 6-*N*-maleimidohexanoic acid and 1.00 µL (0.74 mg; 5.74 µmol) DIPEA in 50 µL DMF. The activated hexanoic acid was added to one half of the residue which was taken up in 50 µL DMF and 5 µL (3.70 mg; 28.7 µmol) DIPEA previously. After 30 min 2.25 mg (1.39 µmol) of the peptide H-Pro-Ala-Ala-Lys-Arg-Val-Lys-Leu-Asp-Lys(DOTA)-Cys-OH was added. After completion the mixture was purified by HPLC. 1.43 mg (0.63 µmol; 66%) of the title compound were obtained after freeze-drying.

LC-MS R_t 9.58 min, m/z 753.0461 $[M+3H]^{3+}$

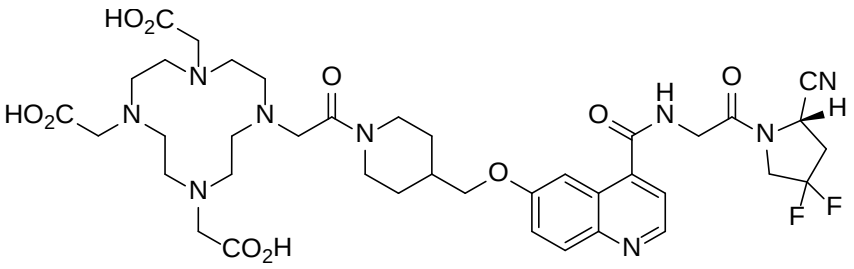

FAPI-11

1.34 mg (1.59 µmol; 74%) were obtained following the general active ester modification protocol.

LC-MS R_t 10.23 min, m/z 844.3358 $[M+H]^{+}$

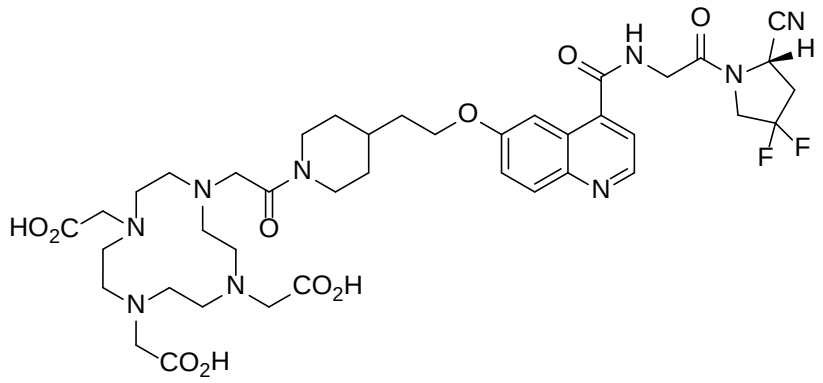

FAPI-12

1.21 mg (1.41 µmol; 67%) were obtained following the general active ester modification protocol.

LC-MS R_t 10.27 min, m/z 858.3506 $[M+H]^+$

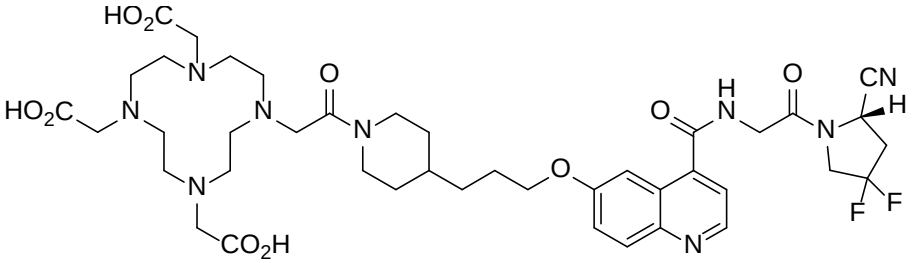

FAPI-13

0.88 mg (1.09 µmol; 65%) were obtained following the general active ester modification protocol.

LC-MS R_t 10.72 min, m/z 872.3726 $[M+H]^+$

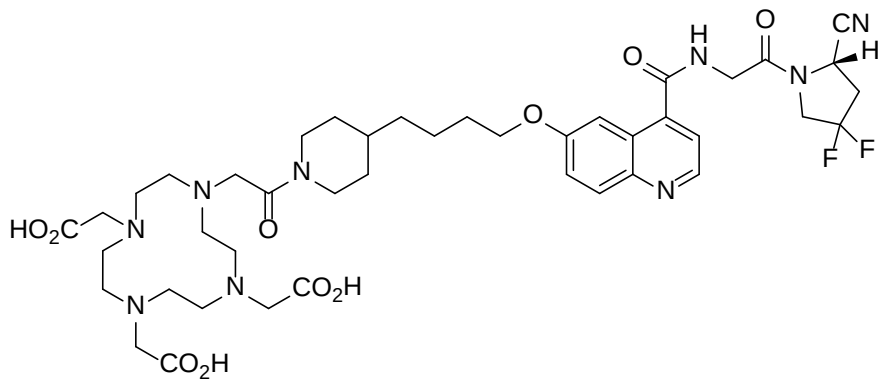

FAPI-14

1.36 mg (1.53 µmol; 83%) were obtained following the general active ester modification protocol.

LC-MS R_t 11.19 min, m/z 886.3874 $[M+H]^+$

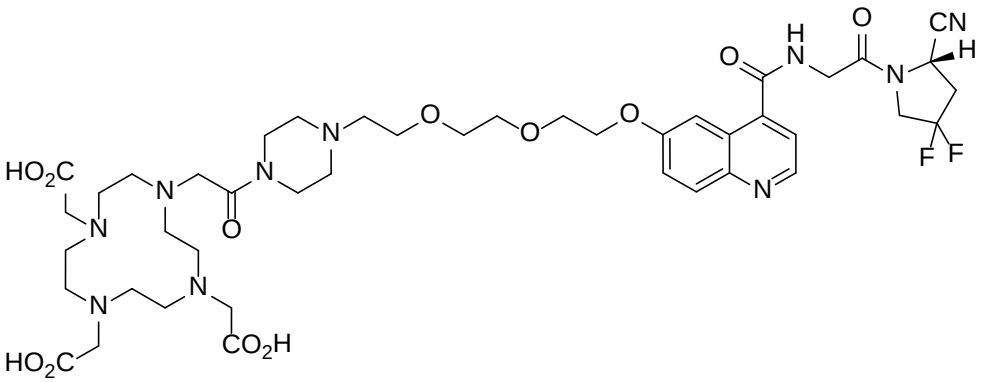

FAPI-15

1.20 mg (1.27 µmol; 89%) were obtained following the general active ester modification protocol.

LC-MS R_t 9.55 min, m/z 947.4001 $[M+H]^+$

SERUM STABILITY

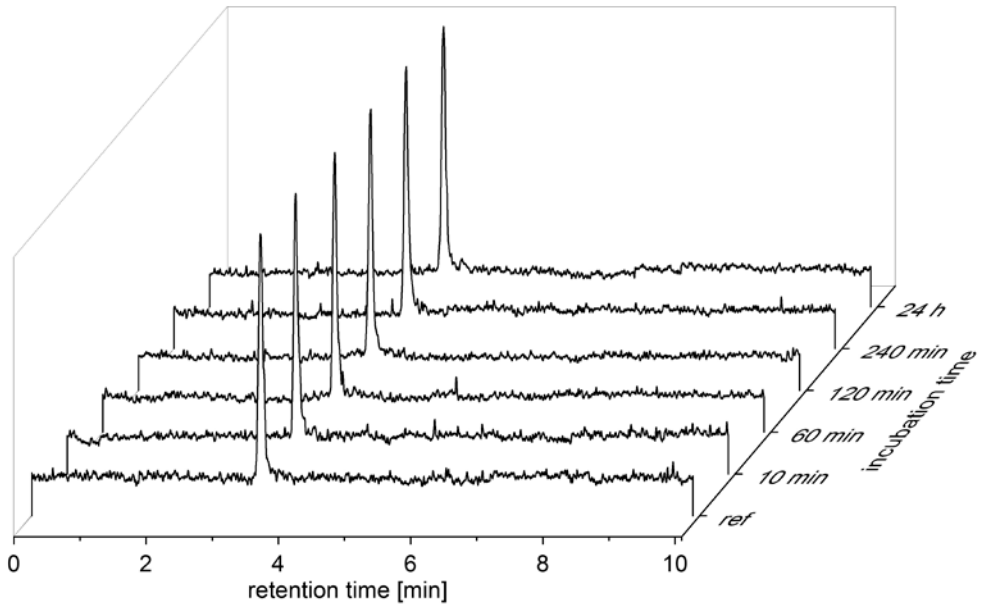

SUPPLEMENTAL FIGURE 2. Stability of ^{177}Lu-FAPI-04 in human serum. Samples were precipitated after the indicated time points and the supernatant subjected to radio-HPLC analysis. Neither free radioactivity nor peaks with different retention time than the reference peak were observed confirming the stability against degradation in human serum.

CELL BASED EXPERIMENTS

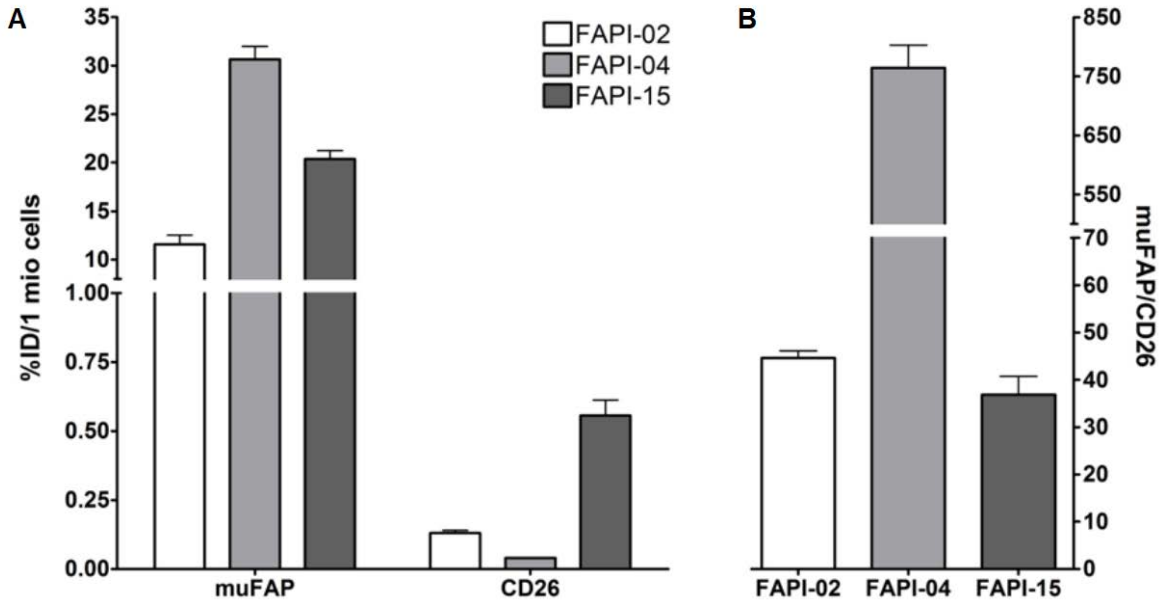

SUPPLEMENTAL FIGURE 3 A. Binding of FAPI derivatives to HEK cells expressing murine FAP-α and human CD26 after 60 min of incubation. B. Ratio of muFAP to CD26 binding.

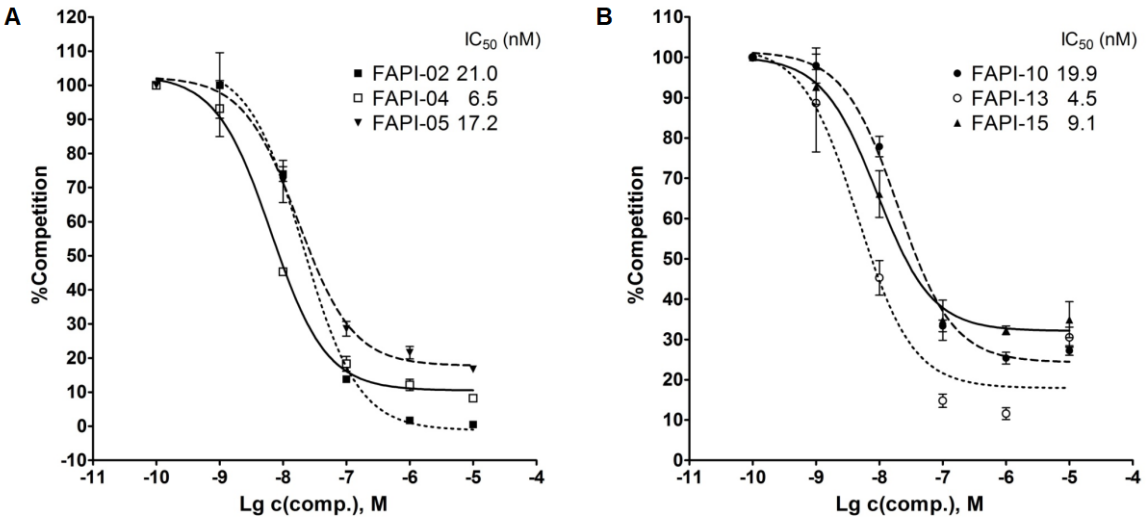

SUPPLEMENTAL FIGURE 4. Competitive binding of selected FAPI derivatives to HT-1080-FAP cells after adding increasing concentrations of unlabeled compound.

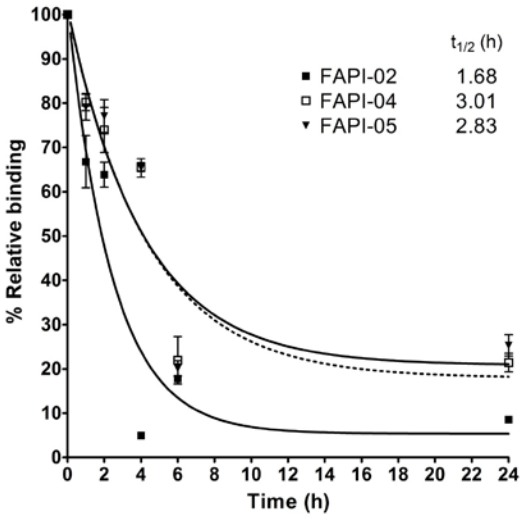

SUPPLEMENTAL FIGURE 5. Efflux kinetics of selected FAPI derivatives after incubation of HT-1080-FAP cells with radiolabeled compound for 60 min and consequent incubation with nonradioactive medium for 1 to 24 hours.

ANIMAL EXPERIMENTS

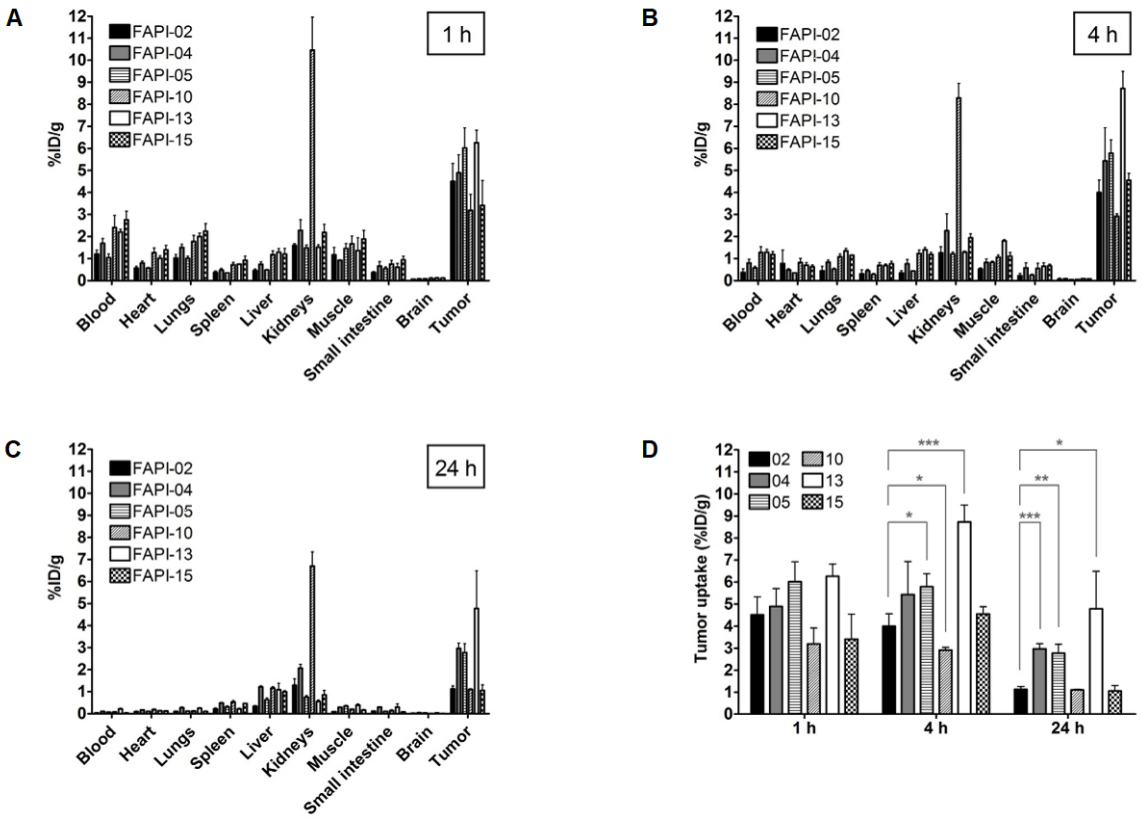

SUPPLEMENTAL FIGURE 6. Biodistribution of all characterized FAPI derivatives in HT-1080-FAP xenotransplants 1 (A), 4 (B) and 24 h (C) after intravenous administration of the radiotracers. D. Tumor uptake of the selected compounds.

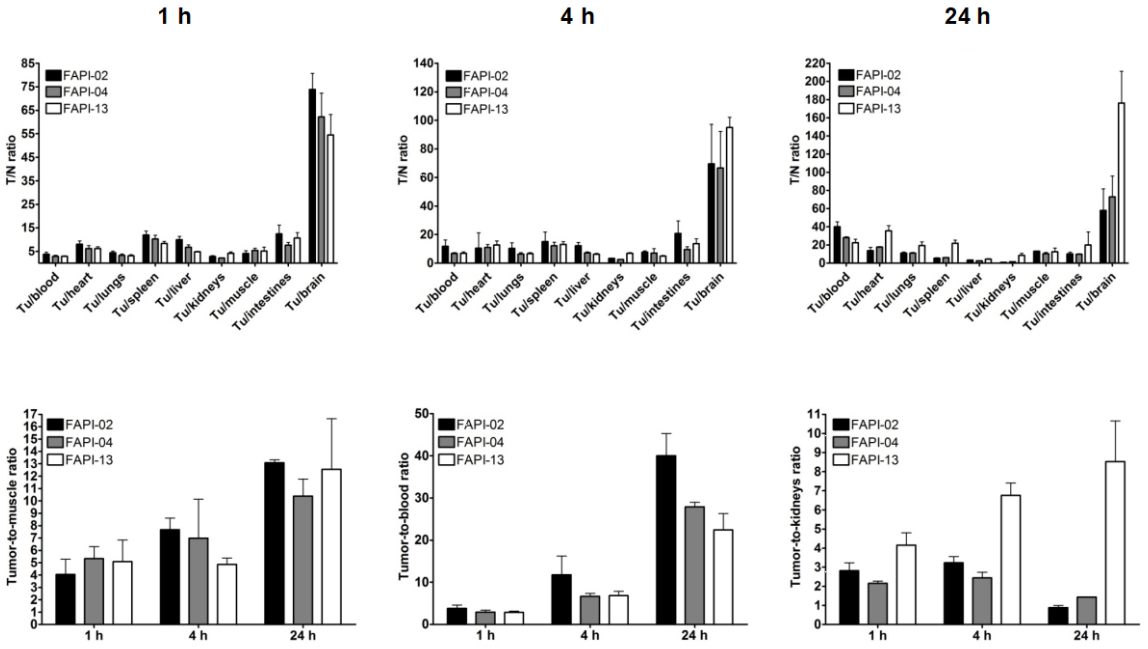

SUPPLEMENTAL FIGURE 7. Tumor-to-organ ratios 1, 4 and 24 h after intravenous injection of selected FAPI derivatives to HT-1080-FAP tumor bearing nude mice, *n = 3.*

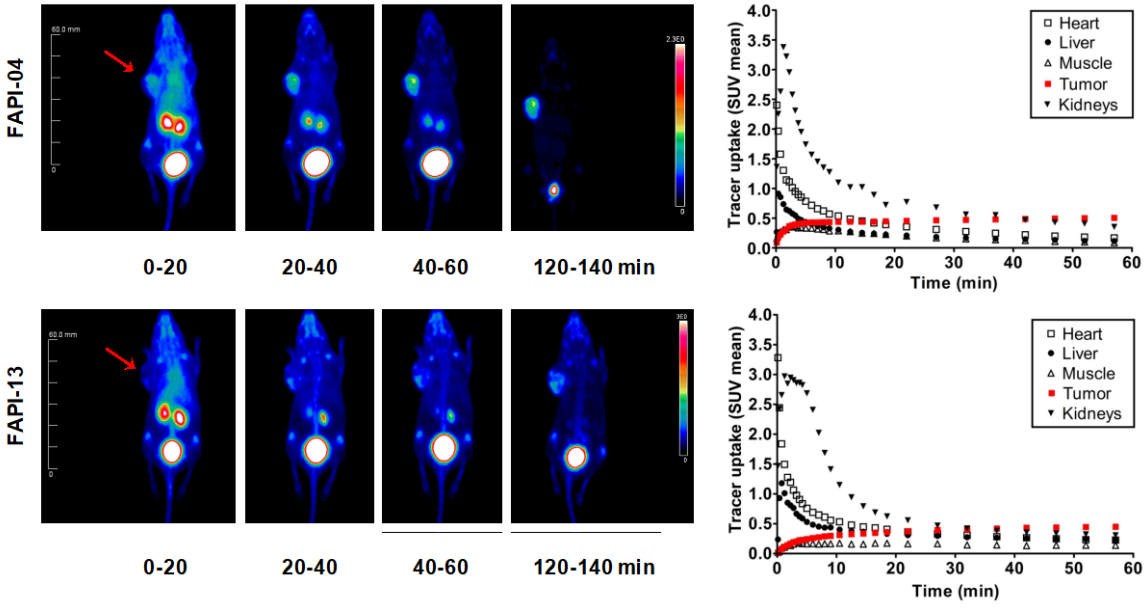

SUPPLEMENTAL FIGURE 8. PET imaging of FAPI-04 and -13 in HT-1080-FAP tumor bearing mice

%ID/g	1 h	4 h	24 h	AUC
FAPI-02	4.5 ± 0.82	4.0 ± 0.56	1.12 ± 0.13	64.0
FAPI-04	4.9 ± 0.82	5.4 ± 1.51	3.0 ± 0.23	99.4
FAPI-05	6.0 ± 0.90	5.8 ± 0.60	2.8 ± 0.40	103.3
FAPI-10	3.2 ± 0.72	2.9 ± 0.12	1.1 ± 0.04	49.3
FAPI-13	6.3 ± 0.57	8.7 ± 0.77	4.8 ± 1.71	157.5
FAPI-15	3.4 ± 1.13	4.6 ± 0.32	1.1 ± 0.25	68.0

SUPPLEMENTAL TABLE 1. Tumor uptake of selected FAPI derivatives in HT-1080-FAP tumor bearing nude mice, *n=3*. Values are reported as percentage of injected dose per gram of tissue (%ID/g; mean ± SD).

Standardized uptake values of FAPI-04 after administration to cancer patients

	Patient 1 (Fig. 5)	Patient 2 (Fig. 6)
Brain	0.10	0.03
Lungs	0.51	0.98
Heart	0.93	1.10
Liver	0.79	1.06
Pancreas	1.08	1.53
Spleen	0.94	1.34
Kidneys	1.18	2.35
Colon	0.83	1.12
Muscle	1.09	1.75
Metastases (average)	9.07	23.86

SUPPLEMENTAL TABLE 2. Maximum tissue uptake (SUV max) 1 h after intravenous administration of ^{68}Ga-FAPI-04 to patients with metastasized breast carcinoma.

REFERENCES

1. Jansen K, Heirbaut L, Cheng JD, et al. Selective Inhibitors of Fibroblast Activation Protein (FAP) with a (4-Quinolinoyl)-glycyl-2-cyanopyrrolidine Scaffold. *ACS Med Chem Lett.* 2013;4:491-496.

2. Jansen K, Heirbaut L, Verkerk R, et al. Extended structure-activity relationship and pharmacokinetic investigation of (4-quinolinoyl)glycyl-2-cyanopyrrolidine inhibitors of fibroblast activation protein (FAP). *J Med Chem.* 2014;57:3053-3074.

3. Loktev A, Lindner T, Mier W, et al. A New Method for Tumor Imaging by Targeting Cancer Associated Fibroblasts. *J Nucl Med.* 2018;in press.

4. Kim SH, Bajji A, Tangallapally R, et al. Discovery of (2S)-1-[4-(2-{6-amino-8-[(6-bromo-1,3-benzodioxol-5-yl)sulfanyl]-9H-purin-9-yl}et hyl)piperidin-1-yl]-2-hydroxypropan-1-one (MPC-3100), a purine-based Hsp90 inhibitor. *J Med Chem.* 2012;55:7480-7501.

5. Mier W, Hoffend J, Kramer S, et al. Conjugation of DOTA using isolated phenolic active esters: the labeling and biodistribution of albumin as blood pool marker. *Bioconjug Chem.* 2005;16:237-240.